NASA TECHNICAL NOTE

NASA TN D-3845

c. 1

LOAN COPY:
AFWL (WLIL-2)
KIRTLAND AFB, N. MEX.

TECH LIBRARY KAFB, NM
0136065

NASA TN D-3845

ROLLING STABILITY DERIVATIVES OF A VARIABLE-SWEEP TACTICAL FIGHTER MODEL AT SUBSONIC AND TRANSONIC SPEEDS

by William P. Henderson, W. Pelham Phillips, and Thomas G. Gainer

Langley Research Center
Langley Station, Hampton, Va.

24 FEB 1967

NATIONAL AERONAUTICS AND SPACE ADMINISTRATION • WASHINGTON, D. C. • FEBRUARY 1967

TECH LIBRARY KAFB, NM
0130665

ROLLING STABILITY DERIVATIVES OF A VARIABLE-SWEEP TACTICAL FIGHTER MODEL AT SUBSONIC AND TRANSONIC SPEEDS

By William P. Henderson, W. Pelham Phillips, and Thomas G. Gainer

Langley Research Center
Langley Station, Hampton, Va.

NATIONAL AERONAUTICS AND SPACE ADMINISTRATION

For sale by the Clearinghouse for Federal Scientific and Technical Information
Springfield, Virginia 22151 – Price $2.50

ROLLING STABILITY DERIVATIVES OF A VARIABLE-SWEEP TACTICAL FIGHTER MODEL AT SUBSONIC AND TRANSONIC SPEEDS

By William P. Henderson, W. Pelham Phillips,
and Thomas G. Gainer
Langley Research Center

SUMMARY

An investigation was made in the Langley high-speed 7- by 10-foot tunnel to determine the rolling stability derivatives of a variable-sweep tactical fighter model. This investigation included the effects of wing sweep, angle of attack, Mach number, and the addition of tail surfaces. The study was made at Mach numbers from 0.40 to 1.20 and at angles of attack from -5° to 20°. The test Reynolds number per foot (per 30.48 cm) varied from 2.45×10^6 to 4.15×10^6. The derivatives presented herein are referred to the stability system of axes and are nondimensionalized with respect to the wing in a 16° sweptback position.

The results indicate that at low angles of attack the wing-fuselage combination exhibited large reductions in the damping-in-roll derivative C_{l_p} and slight decreases in the yawing moment due to rolling velocity C_{n_p} as the wing sweep was increased from 20° to 72.5°. As the angle of attack for the configuration with the wing swept back 20° was increased, the damping in roll was considerably reduced. However, for the configuration with the wings swept back 72.5°, the damping in roll increased for angles of attack from 0° up to about 8°; above this angle-of-attack range, reductions occurred. For the configuration without the wings, the horizontal and vertical tails provided an increment in the damping-in-roll derivative at low angles of attack of about -0.04. With the addition of the wings at either 20° or 72.5° of sweep, this increment was reduced by more than one-half. For all wing sweep angles, the tail assembly contributed a small positive increment to C_{n_p} at zero angle of attack. With increasing angle of attack, this positive contribution decreased and became a negative contribution.

Estimates of the rolling stability derivatives for the wing-fuselage combination were in good agreement with experimental results in the low to moderate angle-of-attack range. The contribution of the tail assembly to the rolling stability derivatives was not accurately predicted.

INTRODUCTION

An extensive research program is being conducted by the National Aeronautics and Space Administration to provide aerodynamic information for airplane configurations employing variable-sweep wings. A number of investigations have indicated that the use of variable sweep offers a means of realizing efficient subsonic and supersonic flight characteristics in one airplane configuration. Recently the study of variable-sweep airplane configurations has been extended to include measurements of the rolling stability derivatives C_{l_p}, C_{n_p}, and C_{Y_p}, which are important to the calculation of the lateral motion of the airplane.

Reference 1 presents measurements of the rolling stability derivatives at subsonic and transonic speeds on a variable-sweep configuration at wing-leading-edge sweep angles of 25°, 75°, and 108°. Also presented in reference 1 is a comparison of experimental and estimated data, made to determine the usefulness of some known methods of estimating these derivatives.

The purpose of the present investigation was to measure the rolling stability derivatives C_{l_p}, C_{n_p}, and C_{Y_p} of a variable-sweep tactical fighter model. Estimates of these derivatives were also made by using the procedures outlined in reference 1, and these estimates are compared with the experimental results. The investigation was made in the Langley high-speed 7- by 10-foot tunnel at Mach numbers from 0.40 to 1.20 and at angles of attack from -5° to 20°. Configurations with wing-leading-edge sweep angles of 20°, 50°, and 72.5° were investigated. Static longitudinal and lateral aerodynamic characteristics of a similar model at subsonic and transonic speeds are presented in references 2 and 3.

SYMBOLS

The results of this investigation are referred to the stability system of axes shown in figure 1. The wind-tunnel data are nondimensionalized with respect to the geometric characteristics of the wing in a 16° sweptback position. These reference dimensions, given both in the U.S. Customary Units and in the International System of Units (SI), are presented in table I. For comparison purposes, the wing area and span for the 20° and 72.5° wings are also presented. The moment reference center was located at fuselage station 23.21 inches (58.95 cm) for the 20° sweptback position and at fuselage station 23.70 inches (60.20 cm) for the 50° and 72.5° sweptback position, as shown in figure 2.

b reference wing span, feet (meters)

$\bar{c}$ mean aerodynamic chord of 16° sweptback wing of configuration A, feet (meters)

C_l rolling-moment coefficient, $\frac{\text{Rolling moment}}{qSb}$

C_n yawing-moment coefficient, $\frac{\text{Yawing moment}}{qSb}$

C_Y side-force coefficient, $\frac{\text{Side force}}{qS}$

$C_{l_p} = \frac{\partial C_l}{\partial\left(\frac{pb}{2V}\right)}$, per radian

$C_{n_p} = \frac{\partial C_n}{\partial\left(\frac{pb}{2V}\right)}$, per radian

$C_{Y_p} = \frac{\partial C_Y}{\partial\left(\frac{pb}{2V}\right)}$, per radian

i_t horizontal-tail incidence angle (positive when trailing edge is down), degrees

M free-stream Mach number

p angular velocity about X stability axis, radians/second

$\frac{pb}{2V}$ wing-tip helix angle, radians

q free-stream dynamic pressure, $\frac{1}{2}\rho V^2$, pounds/foot^2 (newtons/meter^2)

S wing reference area, feet^2 (meters^2)

V free-stream velocity, feet/second (meters/second)

X,Y,Z stability axes

α angle of attack, angle of the wing chord relative to the relative wind, degrees

β angle of sideslip, degrees

Δ increment in a derivative due to tail assembly

Λ leading-edge sweep angle of outboard wing panel, degrees

ρ air density, slugs/foot^3 (kilograms/meter^3)

CONFIGURATION DESIGNATIONS

Two configurations, designated configurations A and B, were tested. Configuration A had a longer fuselage nose length but a shorter wing span than configuration B. (See fig. 2.) The following letter designations are used to represent component parts of the configurations:

F	fuselage
W_{20}	wing with leading edge of outer wing panel swept back 20°
W_{50}	wing with leading edge of outer wing panel swept back 50°
$W_{72.5}$	wing with leading edge of outer wing panel swept back 72.5°
V	vertical tail and ventral fins
H	horizontal tails

MODEL AND APPARATUS

A two-view drawing of the configurations tested is shown in figure 2, and photographs of the model are presented as figures 3 and 4. The wing, which was untwisted, employed NACA 64A-series airfoil sections with 0.20 camber defined parallel to the free stream for the wing in the 16° sweptback position. The thickness for the 16° sweptback wing of configuration A varied from about 11 percent chord at the wing pivot to about 10 percent chord at the wing tip. This wing was mounted at 1° positive incidence relative to the fuselage reference line. The wing for configuration B differs only from the wing for configuration A in that the aspect ratio was increased by extending the wing tips 1.91 inches (4.85 cm) along the span. The 16° sweptback wing is described here because it is the reference wing used to nondimensionalize the data, even though no data were obtained in this investigation for the configurations with the wings in this sweep position. Unless otherwise stated, the inboard glove shown in figure 2 was used on the wing.

The horizontal tails had a modified biconvex airfoil section (parallel to free stream) with a thickness of 4 percent chord at the root and 3 percent chord at the tip. These tails, when rotated about a hinge line which was swept back 13.3°, were capable of deflection angles from 0° to -20°. The vertical tail section consisted of a 4-percent-thick modified biconvex airfoil (parallel to the free stream).

All tests were made with the inlets open and the inlet spike positioned to provide the proper engine airflow at a Mach number of 1.20.

A sketch of the steady-state forced-roll apparatus installed in the Langley high-speed 7- by 10-foot tunnel is shown in figure 5. The model was

mounted on a six-component wire strain-gage balance of the type normally used for static tests of sting-supported models. Electrical signals from the strain-gage balance were transmitted to the data recording equipment by wire leads, slip rings, and brushes. Variation of angle of attack was obtained by means of interchangeable couplings between the balance and the rotating sting support. A more complete description of the mechanical operation of this apparatus is presented in reference 1.

TESTS AND CORRECTIONS

Damping-in-roll tests were made in the Langley high-speed 7- by 10-foot tunnel over a Mach number range from 0.40 to 1.20 for the 72.5° wing sweep position and from 0.40 to 0.80 for the 20° wing sweep position. The angle of attack was varied from -5° to 20°. The variation of the test Reynolds number per foot (per 30.48 cm) with Mach number is presented in figure 6.

The support system deflected under load and these deflections, combined with the effects of model product of inertia and any initial displacement of the center of mass of the model from the roll axis, introduced centrifugal forces and moments when the model was rotated. The contribution of these centrifugal forces and moments to C_l, C_n, and C_Y are, to the first order, symmetrical about zero rolling velocity. The rolling derivatives C_{l_p}, C_{n_p}, and C_{Y_p} were therefore reduced from data obtained at several rolling velocities having equal magnitude but opposite sign so that the centrifugal contribution would be canceled. The angles of attack have also been corrected for deflection of the balance and support system under load.

In an attempt to fix transition, 0.10-inch-wide (0.254-cm) strips of No. 120 carborundum grains (mean particle diameter of 0.0049 inch (0.0124 cm)) were placed on the model. These strips were applied around the fuselage 1.65 inches (4.19 cm) back from the nose, around the inlets 0.40 inch (1.01 cm) from the leading edge, and at 0.25 inch (0.64 cm) rearward perpendicular to the leading edges of the wing, horizontal tails, and vertical tails.

For all tests at transonic speeds ($M > 0.80$) with the open-slot configuration of the tunnel, no jet-boundary or blockage corrections are necessary and therefore were not applied to the data. However, for the tests at subsonic speeds, with the closed-slot configuration of the tunnel, jet-boundary corrections estimated using reference 4 were applied to the angle of attack, and blockage corrections estimated using reference 5 were applied to the dynamic pressure and Mach number.

PRESENTATION OF DATA

The derivatives presented herein are referred to the stability system of axes and are nondimensionalized with respect to the wing in a 16° sweptback

position. For convenience in locating a particular set of data, the following outline of the contents of the data figures is presented:

RESULTS AND DISCUSSION

Experimental Results

The basic data of this investigation were obtained as the variation of forces and moments with wing-tip helix angle $pb/2V$ at each test Mach number and angle of attack. The derivatives C_{l_p}, C_{n_p}, and C_{Y_p} were then extracted from these data at values of $pb/2V$ of equal magnitude but opposite sign. Results with different data symbols were obtained at different values of angular velocity. In general, rolling velocity is seen to have only a slight effect on the rotary stability derivatives in the low angle-of-attack range. (For example, see fig. 8.) However, at the higher angles of attack, where wing stall

is encountered, rolling velocity is seen to have a significant effect on these derivatives.

The effect of the wing glove on the rotary stability derivatives for configuration A with the wing swept back 20° can be seen by comparing figure 7 with figure 8. These data indicate that the wing glove generally has no effect on any of these derivatives. This result is to be expected since the area, as well as the aspect ratio, of the wing glove is small as compared with that of the unswept wing outer panel.

Figures 8, 15, and 18 together with figures 12, 16, and 22 show that at low angles of attack large reductions in the damping in roll (negative values of C_{l_p} indicate positive damping) occur as the wing sweep of configuration A is increased from 20° to 72.5°. This reduction in C_{l_p} results from the decreased lifting capabilities exhibited by the wing as the wing sweep is increased and the aspect ratio is reduced and is emphasized by the fact that a constant wing span was used for the coefficients. As previously mentioned, the derivatives presented in this paper are nondimensionalized with respect to the 16° sweptback wing. Although this procedure results in a greater variation of C_{l_p} with sweep angle than would occur if the wing dimensions appropriate to each sweep angle had been used for reference, the procedure used reflects correctly the effect of sweep on the damping moment produced by a given roll rate.

Figure 12 indicates that as the angle of attack for the configuration without the tail surfaces and with the wings swept back 20° is increased the damping in roll is considerably reduced, even to the point of having zero damping at the higher angles of attack. This reduction in damping in roll with increasing angle of attack is the result of separation on the movable portion of the wing. As shown in reference 6, this wing separation can be significantly reduced by the use of leading-edge high-lift devices. For the 72.5° sweptback wing (fig. 22), the damping in roll increases as the angle of attack is increased from 0° up to about 8°; above this angle-of-attack range, reduction in the damping in roll is evident. The increase in the damping in roll is directly related to the increase in the lift-curve slope exhibited by highly swept, low-aspect-ratio wings over this angle-of-attack range.

The contribution of the horizontal and vertical tails to the damping in roll for configuration A with the wings swept back 20° can be seen by comparing figure 8 with figure 12; with the wings swept back 72.5°, figure 18 with figure 22; and without the wing, figure 24 with figure 25. The data are summarized for low angles of attack in figure 27. These data indicate that for the configuration without the wings, the horizontal and vertical tails provide an increment in the damping-in-roll derivative C_{l_p} at low angles of attack of about -0.04. The addition of the wings to the configuration at either 20° or 72.5° of sweep produces interference on the tail surfaces, which results in the damping-in-roll contribution of the tails being reduced by more than one-half. Increasing the angle of attack of the configuration from 0° to 20° results in approximately doubling the damping-in-roll contribution of the tail surfaces. (Compare fig. 8 with fig. 12 and fig. 18 with fig. 22.)

A comparison of the stability derivatives for configurations A and B with the wings swept back 20° can be seen by comparing figure 8 with figure 14. These data indicate that at low angles of attack configuration B, which has a higher aspect ratio wing than configuration A, exhibits higher values of roll damping (more negative values of C_{l_p}). However, at a sweep angle of 72.5° (compare fig. 18 with fig. 23), configuration B has less negative values of C_{l_p} than does configuration A. These less negative values of C_{l_p} exhibited by configuration B with its wings swept back 72.5° result from the fact that for low-aspect-ratio wings the damping depends primarily on the wing span and that the increase in wing span of configuration B over configuration A (with the wings swept back 72.5°) is less than the increase in the product of the reference area and span used in nondimensionalizing the coefficients. If, on the other hand, the damping-in-roll derivatives had been based on the total area and span of the 72.5° sweptback-wing—horizontal-tail combination, the values of C_{l_p} for configuration B would be slightly more negative than those for configuration A. The damping moment produced by a given roll rate is increased significantly by the added length to the wing tips of configuration B for all sweep angles.

The variations of C_{n_p} and C_{Y_p} with Mach number for the test values of angle of attack and wing-tip helix angle are also presented in the data figures for the various configurations investigated. These data indicate that with the tail surfaces removed, negative values of C_{n_p} were observed at low angles of attack for the configurations, and these values decreased slightly with increasing wing sweep. (For example, see figs. 12, 16, 22, and 28.) For the configuration with the wings swept back 72.5°, C_{n_p} varies only slightly with increasing angle of attack. (See figs. 22 and 28.) However, for the configuration with the wings swept back 20°, the variation of C_{n_p} with angle of attack is somewhat more pronounced, in that negative values of C_{n_p} were obtained at low and high angles of attack, and positive values in the intermediate angle-of-attack range. (See figs. 12 and 28.)

For all wing sweep angles, the tail surfaces contributed a small positive increment to C_{n_p} at zero angle of attack. (See fig. 29.) With increasing angle of attack, the positive contribution of the tails to C_{n_p} decreased and became a negative contribution, with the angle at which the C_{n_p} becomes negative being dependent on the wing sweep.

Estimation of Derivatives

Estimates have been made of some of the rolling stability derivatives for comparison with the experimental results. Since the methods used for these estimates are described in detail in reference 1, only the more pertinent parts pertaining to the methods of estimations and the results will be discussed herein.

The damping-in-roll derivative C_{l_p} was estimated for two wings representative of the model wing of configuration A at sweep angles of 20° and 72.5°. Geometric parameters of the two simplified wing planforms used in the estimates are as follows:

Wing	Wing span		Wing area		Aspect ratio	Taper ratio	Quarter-chord sweep angle, deg
	ft	cm	ft^2	cm^2			
W_{20}	2.81	85.65	1.086	1009	7.30	0.33	16.5
$W_{72.5}$	1.47	44.81	1.288	1197	1.67	.30	70.0

In order to compare the estimates with the experimental data, the estimated values of the rolling stability derivatives were converted so as to be based on the reference dimensions used for configuration A. The planform used to represent wing W_{20} was obtained by simply extending the outer panel leading and trailing edges into the plane of symmetry. No attempt was made to account for the additional area of the inboard glove for the configuration with the 20° sweptback wing. The simplified $W_{72.5}$ planform had a streamwise tip with the wing having the same area and aspect ratio as the wing of the configuration.

The damping-in-roll derivatives were estimated for the two wings and are compared with the experimental results in figures 12 and 22 for the 20° and 72.5° sweptback-wing positions, respectively. These data indicate that good agreement exists between the experimental and estimated values of the damping in roll for both sweptback-wing positions at angles of attack up to 8°. Above this angle of attack, the method considerably overestimates the damping in roll. This overestimation of C_{l_p} can be explained in that the angle-of-attack correction to the estimated damping-in-roll derivative C_{l_p} is the ratio of the lift-curve slope for the wing at the angle of attack of interest to the lift-curve slope at an angle of attack of 0°, as explained in reference 1. Since no wing-alone static data were available for these wing planforms, the ratio of the lift-curve slopes was obtained from static data for the wing-body combination (refs. 2 and 3). The fuselage, because of its nonlinear lift-curve slope, has a considerable contribution to the lift-curve slope of the wing-body combination at high angles of attack and only a very slight contribution to the C_{l_p}.

The experimentally determined contribution of the horizontal tails to C_{l_p} is compared in figure 26 with values estimated for the horizontal tails isolated from the rest of the configuration. The data of figure 26 indicate that the estimate for the isolated horizontal tails is considerably higher than the experimental contribution of the horizontal tails. This can possibly be attributed to the effects of the flow field generated by the wings and the fuselage on the horizontal tails. No attempt was made to account for this effect.

Figure 27 shows the experimental contribution of the complete tail assembly to C_{l_p} for the configuration with the wings swept back 20° and 72.5° and for

the configuration without the wings. These data are also compared with the values estimated for the isolated horizontal tails. The experimental contribution of the tail assembly to C_{l_p} for the configuration without the wings, as would be expected, is higher (more negative values of C_{l_p}) than that estimated for the isolated horizontal tails. However, with the addition of the wings at either sweepback angle, a considerable reduction in the contribution of the tail assembly to C_{l_p} is noted, with these experimental values being lower (less negative) than those estimated for the isolated horizontal tails.

The estimated variation of C_{n_p} with Mach number and angle of attack for the 20° and 72.5° wings is compared with the experimental wing-fuselage results in figures 12, 22, and 28. These data show good agreement between estimated and experimental results in the angle-of-attack range between 0° and 13° for the 20° sweptback wing, and over the entire test angle-of-attack range for the 72.5° sweptback wing. The procedure for estimating C_{n_p} for the wing-body combination uses as one of its inputs the estimated value of C_{l_p} for the wing. Since in the high angle-of-attack range the estimated values of C_{l_p} for the wing-body combination are generally higher than the experimental values, the experimental and estimated values of C_{n_p} also do not agree. However, when the experimental values of C_{l_p} are used, the trends in the variation of C_{n_p} with angle of attack can better approximate the experimental variation.

The estimated and experimental contributions of the tail assembly to C_{n_p} and C_{Y_p} are presented as functions of angle of attack in figure 29. The estimates made use of theoretical characteristics of intersecting tail surfaces presented in reference 7. At an angle of attack near 0°, the estimated results agree fairly well with the experimental results. However, with increasing angle of attack, the slopes of the measured tail contribution were considerably higher than the estimated slopes for the isolated tail assembly. These results are probably due to interference effects from the wing and fuselage on the tail assembly, and also to the tail assembly itself – that is, the actual planform of the tails could not be closely approximated by the tail assemblies considered in reference 7.

SUMMARY OF RESULTS

An investigation to determine the rolling stability derivatives of a variable-sweep tactical fighter model indicated the following results. The derivatives presented herein are referred to the stability system of axes and are nondimensionalized with respect to the wing in a 16° sweptback position.

1. At low angles of attack the wing-fuselage combination exhibited large reductions in the damping-in-roll derivative C_{l_p} and slight decreases in the

yawing moment due to rolling velocity C_{n_p} as the wing sweep angle was increased from 20° to 72.5°.

2. As the angle of attack for the wing-fuselage configuration with the wings swept back 20° was increased, the damping in roll was considerably reduced. However, for the configuration with the wings swept back 72.5°, the damping in roll increased for angles of attack from 0° up to about 8°; above this angle-of-attack range, reductions occurred.

3. For the configuration without the wings, the horizontal and vertical tails provided an increment in the damping-in-roll derivative at low angles of attack of about -0.04. With the addition of the wings at either 20° or 72.5° of sweep, this increment was reduced by more than one-half.

4. For all wing sweep angles, the tail assembly contributed a small positive increment to C_{n_p} at zero angle of attack. With increasing angle of attack, the positive contribution decreased and became a negative contribution.

5. Estimates of the rolling stability derivatives for the wing-fuselage combination were in good agreement with experimental results in the low to moderate angle-of-attack range.

6. The contribution of the tail assembly to the rolling stability derivatives was not accurately predicted.

Langley Research Center,
National Aeronautics and Space Administration,
Langley Station, Hampton, Va., September 22, 1966,
126-13-02-21-23.

REFERENCES

1. Hayes, William C., Jr.; Kemp, William B., Jr.; and Thompson, Wilson E.: Wind-Tunnel Measurements and Estimated Values of the Rolling Stability Derivatives of a Variable-Sweep Airplane Configuration at Subsonic and Transonic Speeds. NASA TM X-600, 1961.

2. Ayers, Theodore G.: Transonic Aerodynamic Characteristics of a Variable-Wing-Sweep Tactical Fighter Model – Phase 1. NASA TM X-1039, 1964.

3. Ayers, Theodore G.: Transonic Aerodynamic Characteristics of a Variable-Wing-Sweep Tactical Fighter Model – Phase 2. NASA TM X-1040, 1964.

4. Gillis, Clarence L.; Polhamus, Edward C.; and Gray, Joseph L., Jr.: Charts for Determining Jet-Boundary Corrections for Complete Models in 7- by 10-Foot Closed Rectangular Wind Tunnels. NACA WR L-123, 1945. (Formerly NACA ARR L5G31.)

5. Herriot, John G.: Blockage Corrections for Three-Dimensional-Flow Closed-Throat Wind Tunnels, With Consideration of the Effect of Compressibility. NACA Rept. 995, 1950. (Supersedes NACA RM A7B28.)

6. Hassell, James L., Jr.: Low-Speed Flight Characteristics of a Variable-Wing-Sweep Fighter Airplane Model. NASA TM X-1036, 1965.

7. Queijo, M. J.; and Riley, Donald R.: Calculated Subsonic Span Loads and Resulting Stability Derivatives of Unswept and 45° Sweptback Tail Surfaces in Sideslip and in Steady Roll. NACA TN 3245, 1954.

TABLE I

WING AREA AND SPAN DIMENSIONS FOR THE TWO CONFIGURATIONS

AT SEVERAL WING SWEEP ANGLES

Configuration	Wing area		Wing span	
	ft^2	cm^2	in.	cm
$\Lambda = 16^\circ$ (reference wing)				
A	1.085	1008	34.364	87.285
B	1.136	1055	38.182	96.982
$\Lambda = 20^\circ$				
A	1.086	1009	33.764	85.761
B	1.137	1056	37.527	95.319
$\Lambda = 72.5^\circ$				
A	1.288	1197	17.620	44.755
B	1.339	1244	18.610	47.269

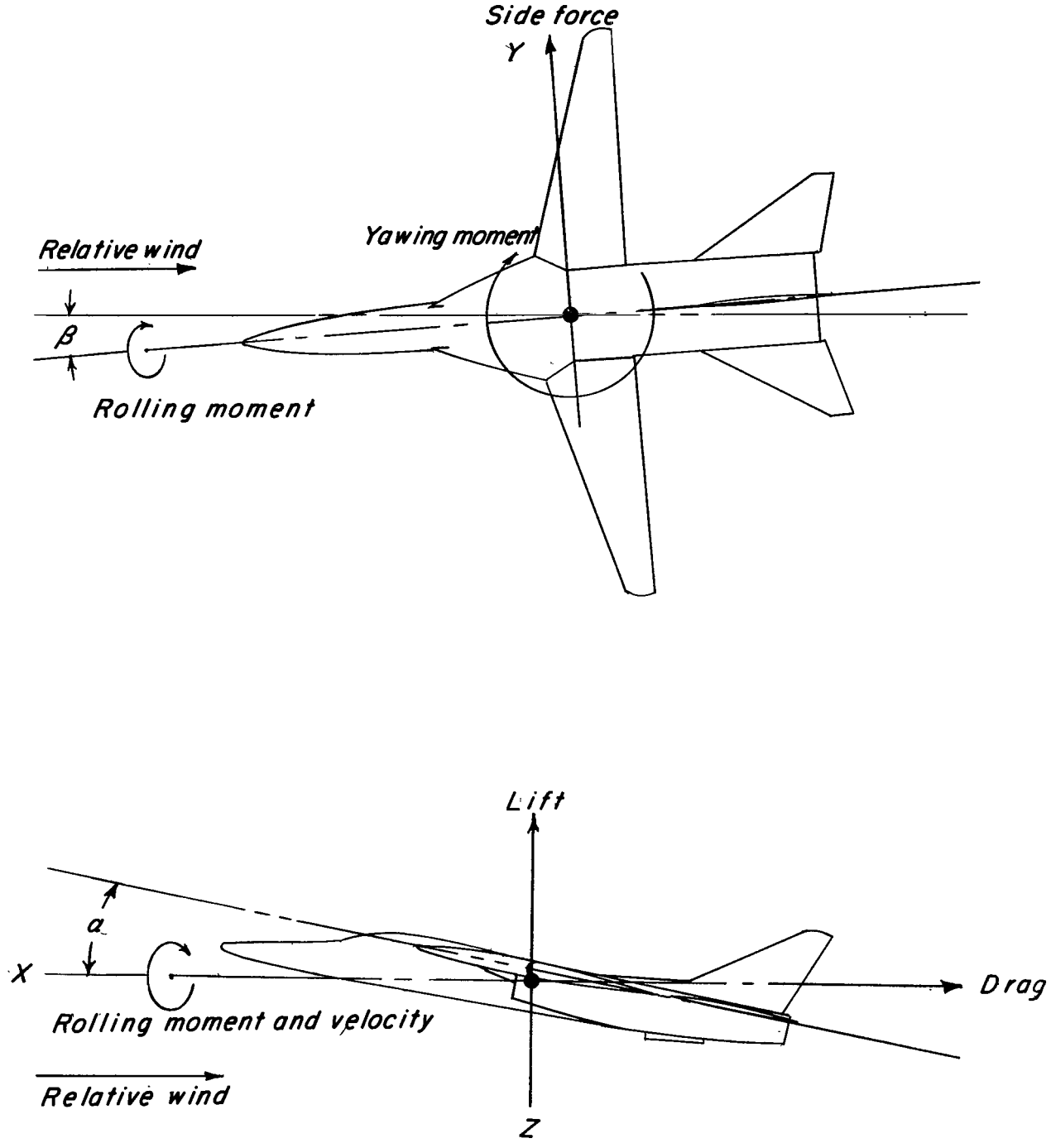

Figure 1.- Stability system of axes showing positive direction of forces, moments, angles, and velocities.

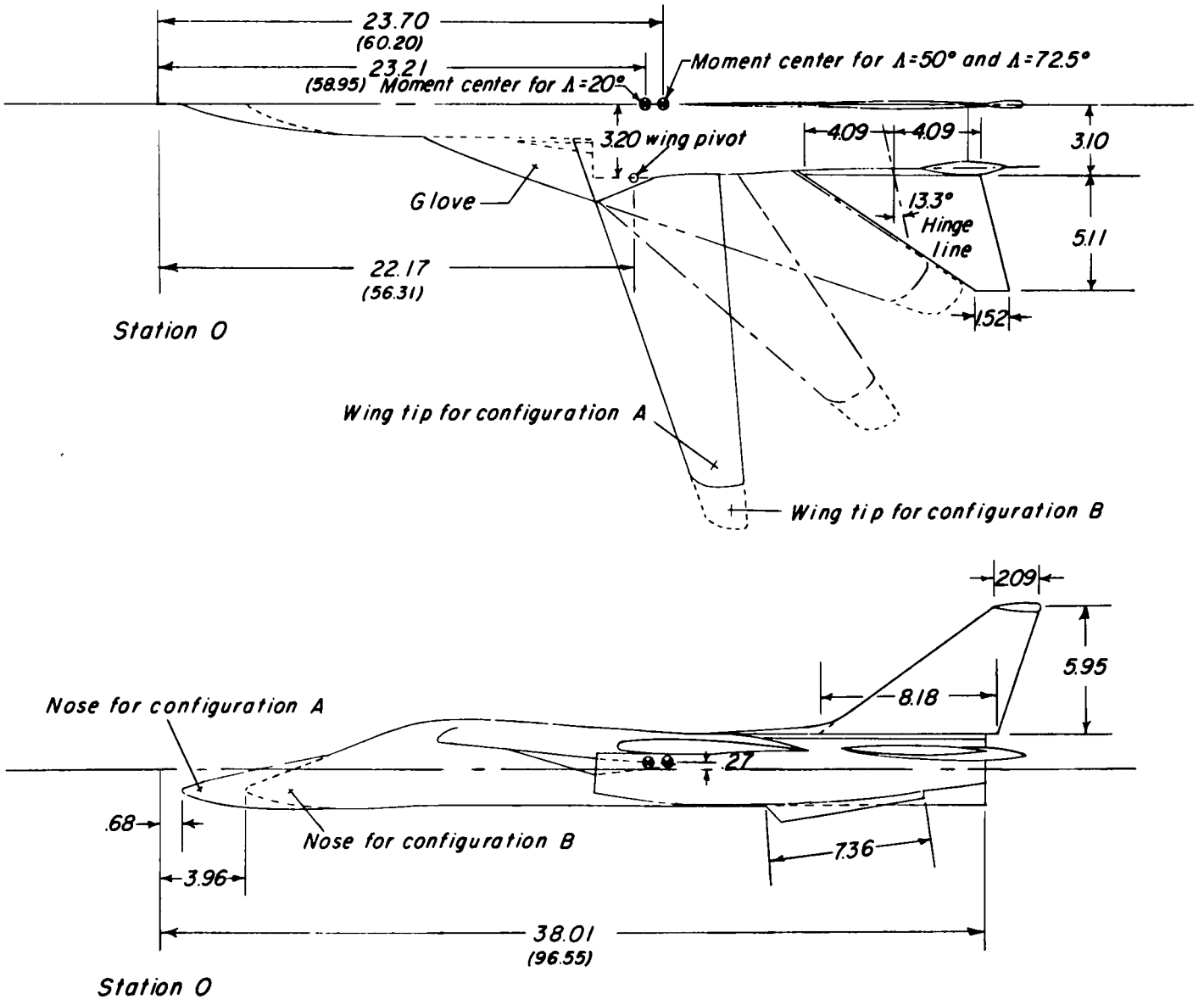

Figure 2.- Details of configurations. Dimensions are given first in inches and parenthetically in centimeters; however, because of space limitations, conversions to the International System of Units are not presented for all dimensions.

Figure 3.- Photograph of model mounted on steady-state roll apparatus in the 7- by 10-foot tunnel. L-63-7912

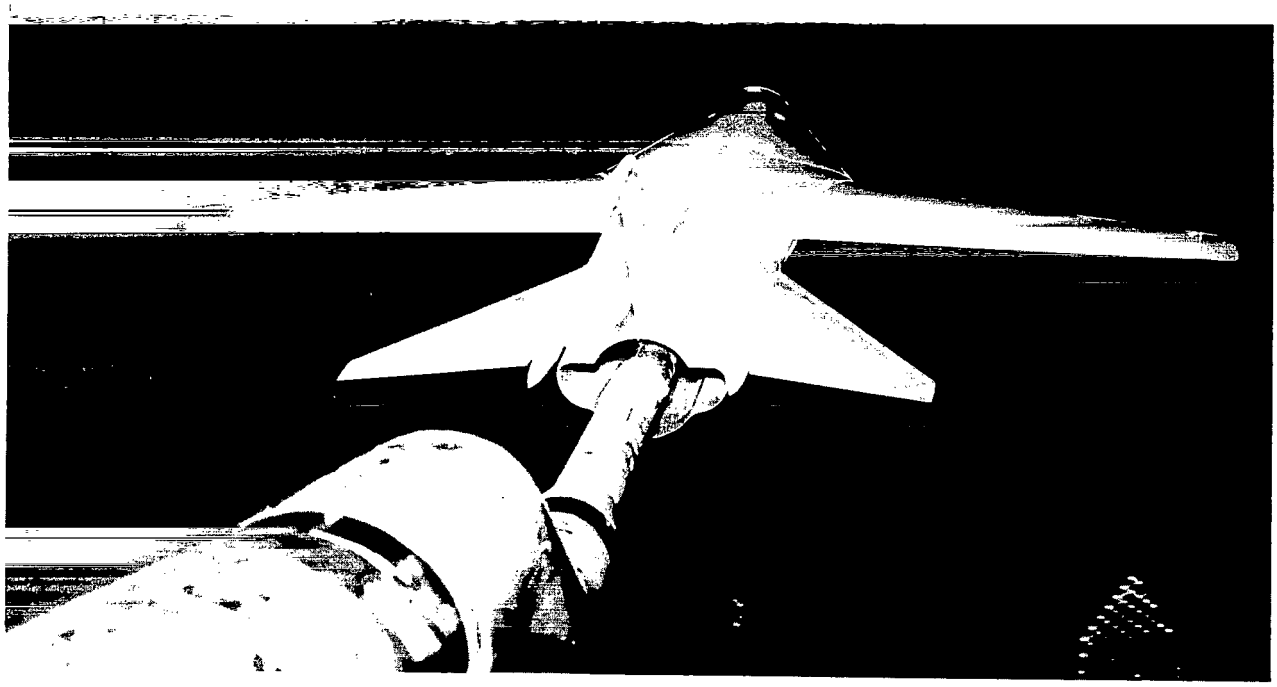

(a) Configuration A; $\Lambda = 20^{\circ}$. L-63-7913

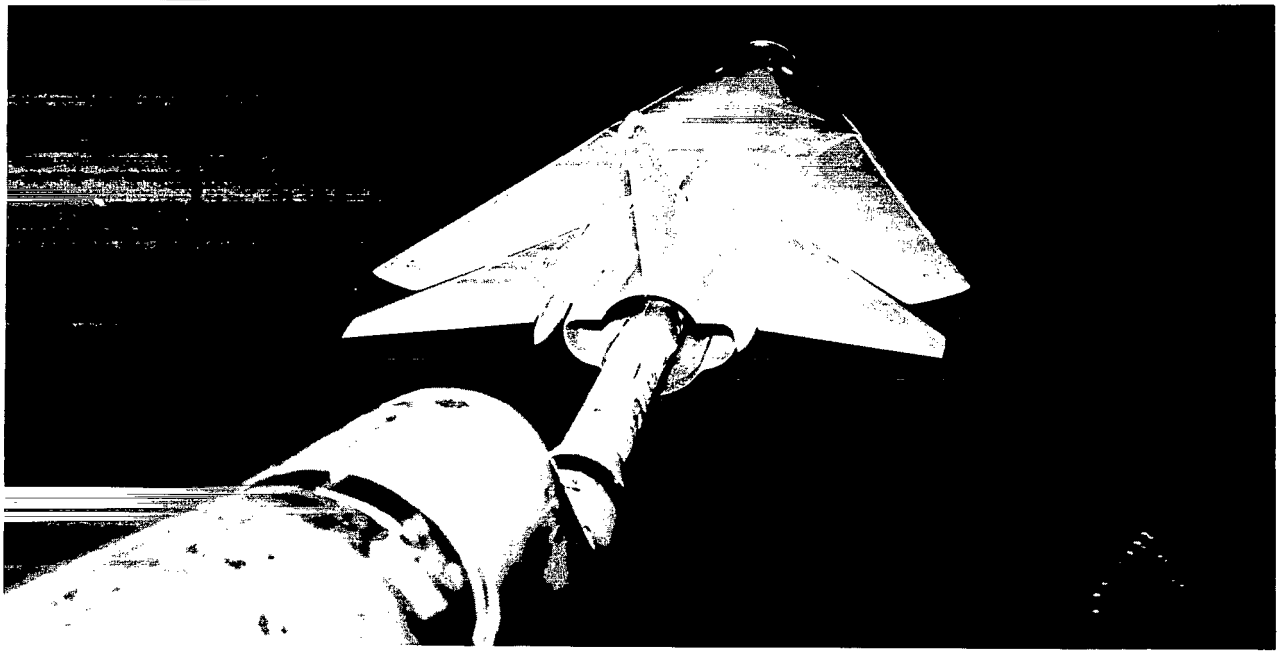

(b) Configuration A; $\Lambda = 72.5^{\circ}$. L-63-7910

Figure 4.- Photographs of model in Langley high-speed 7- by 10-foot tunnel.

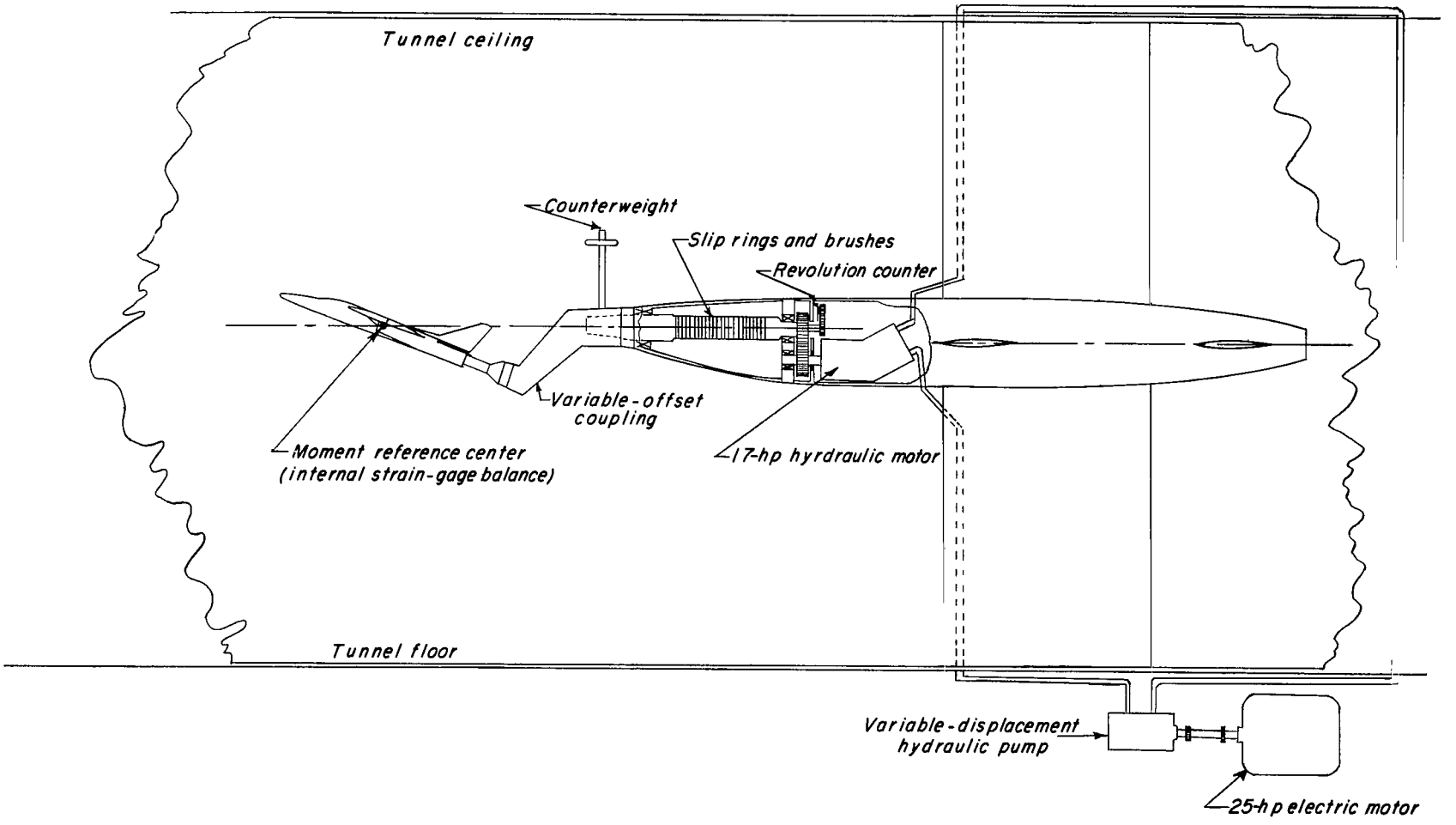

Figure 5.- General arrangement of forced-roll apparatus installed in the Langley high-speed 7- by 10-foot tunnel.

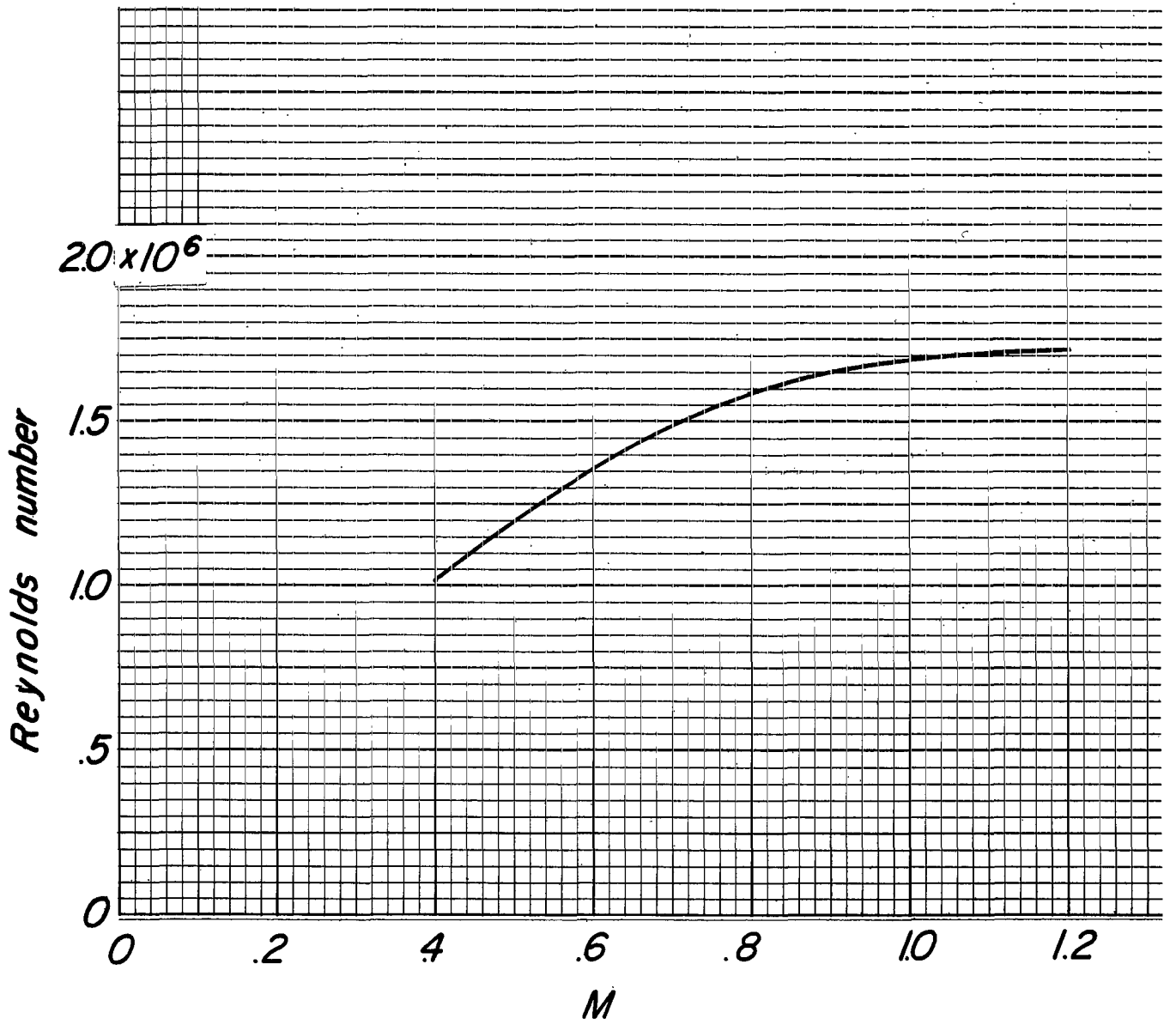

Figure 6.- Variation of Reynolds number with Mach number (based on $\bar{c}$ of configuration A).

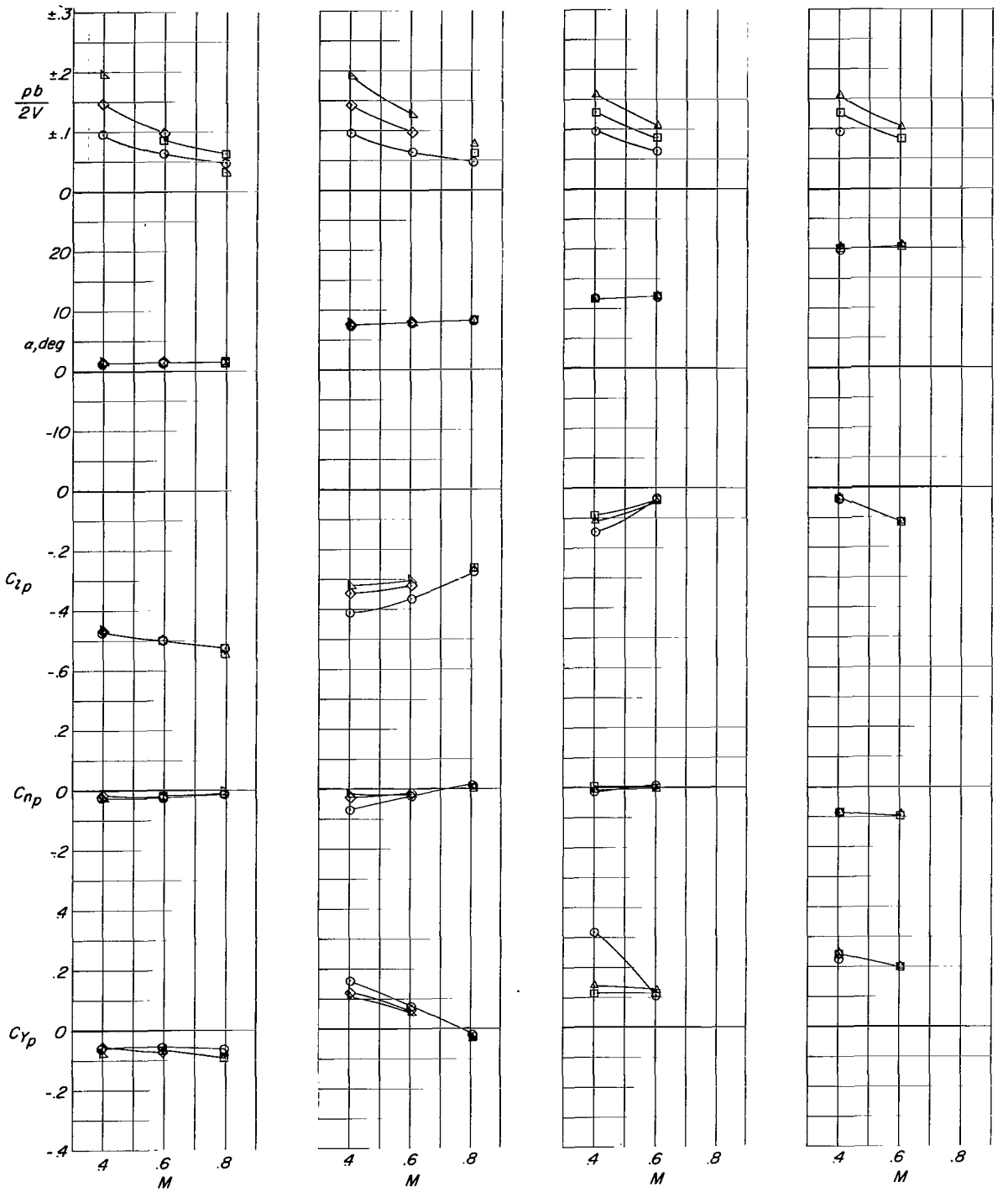

Figure 7.- Variation of rolling stability derivatives with Mach number for configuration A with $FW_{20}VH$ and glove off. $i_t = 0^o$.

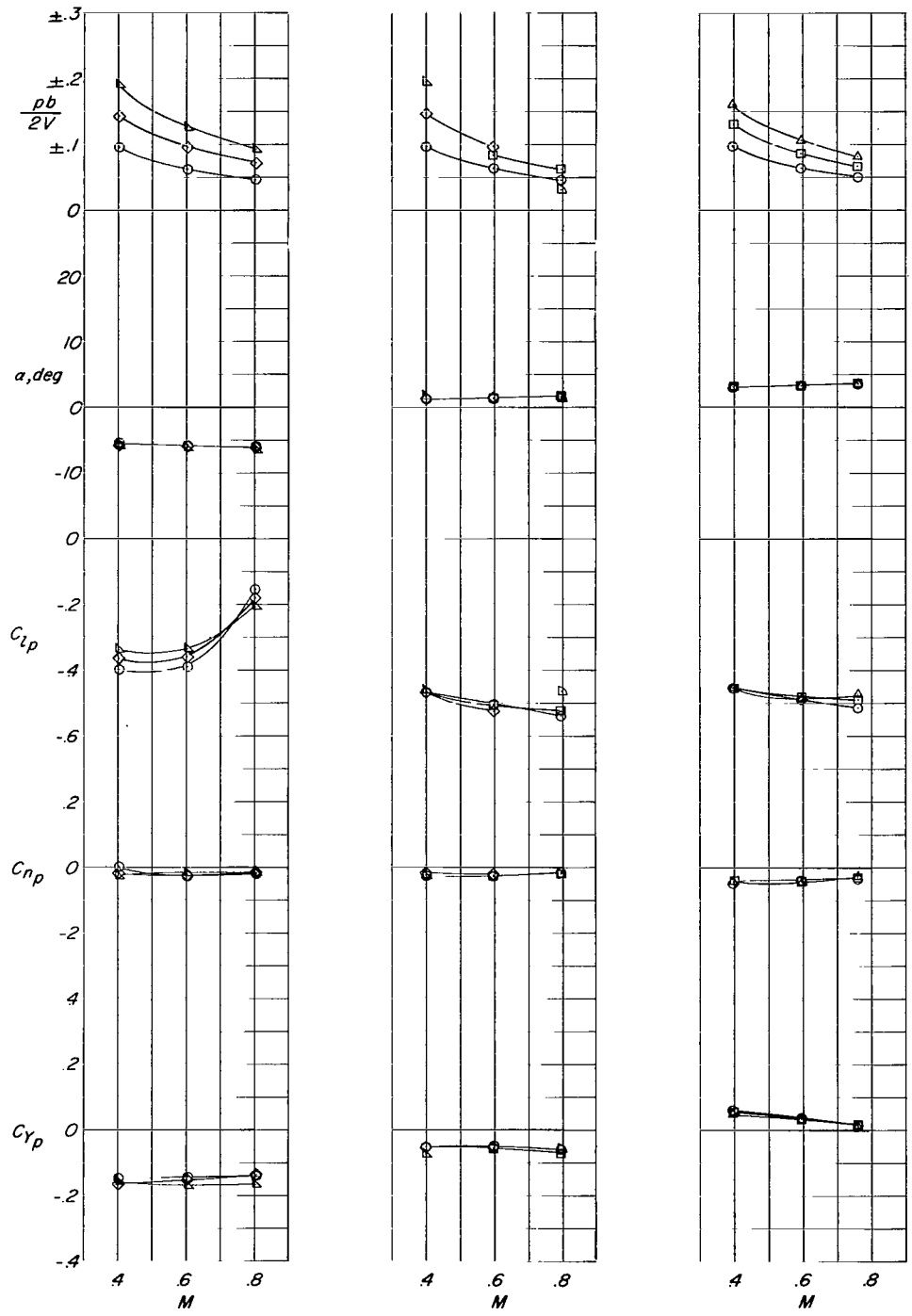

Figure 8.- Variation of rolling stability derivatives with Mach number for configuration A with $FW_{20}VH$. $i_t = 0^o$.

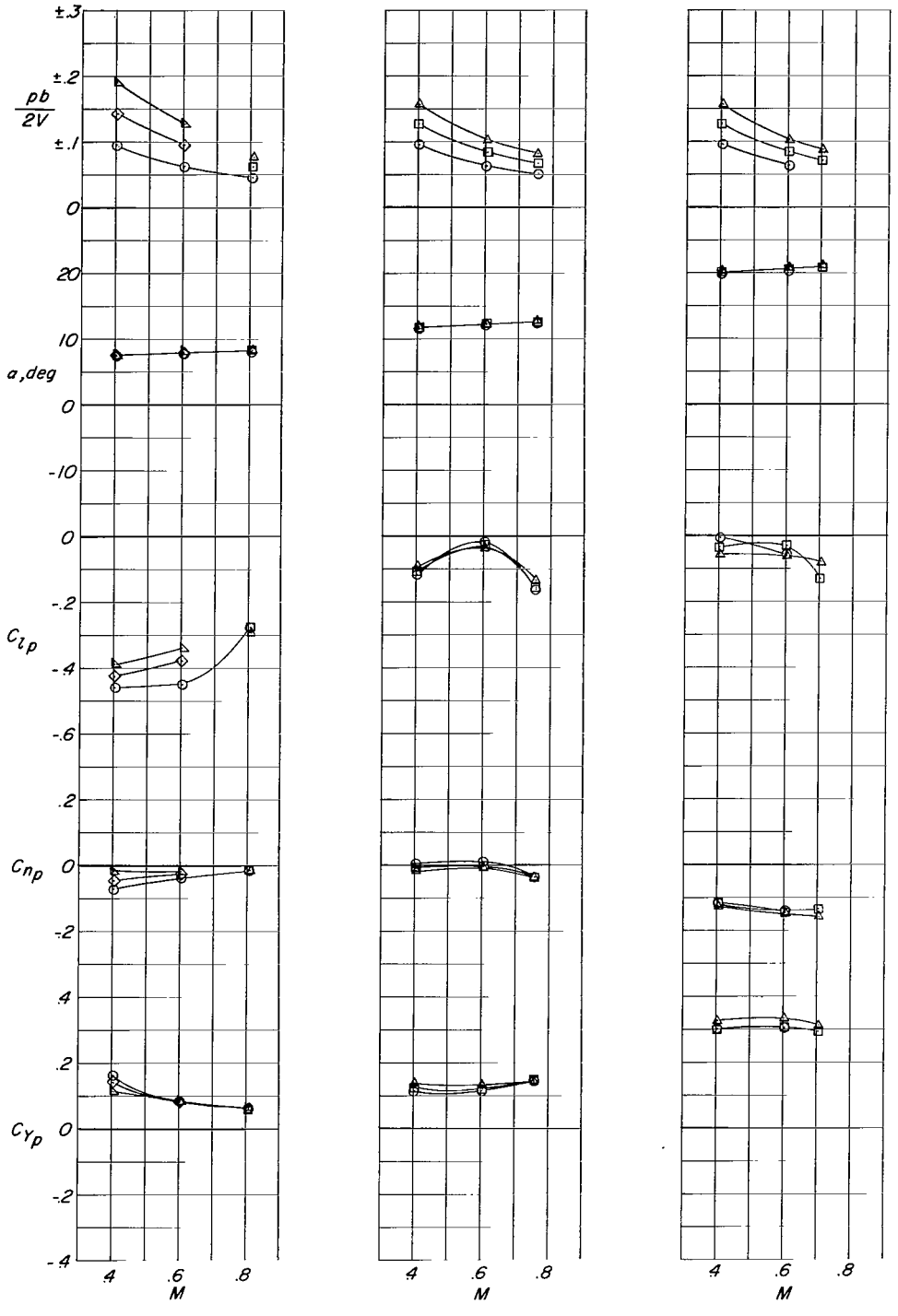

Figure 8.- Concluded.

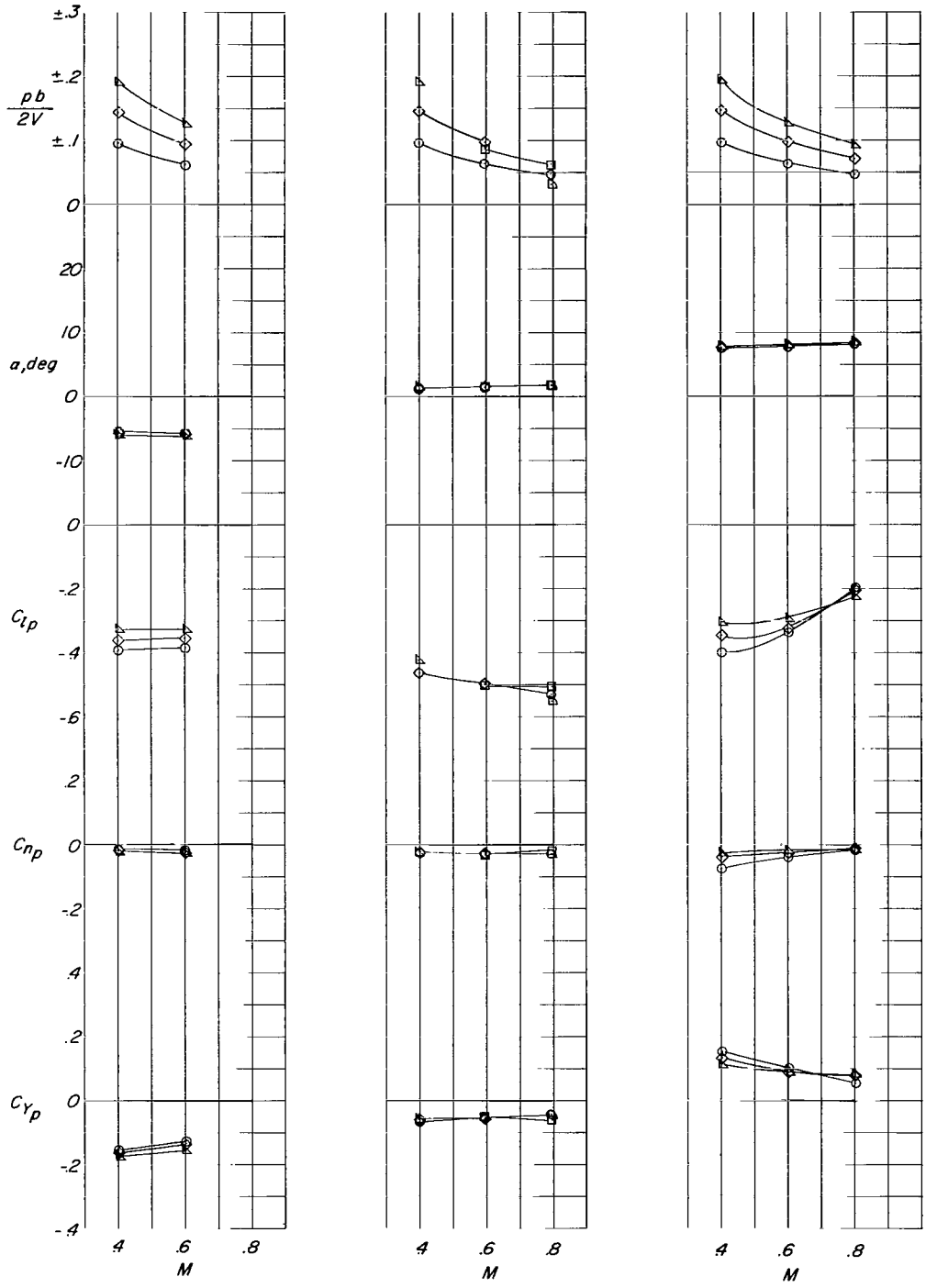

Figure 9.- Variation of rolling stability derivatives with Mach number for configuration A with $FW_{20}VH$. $i_t = -10^0$.

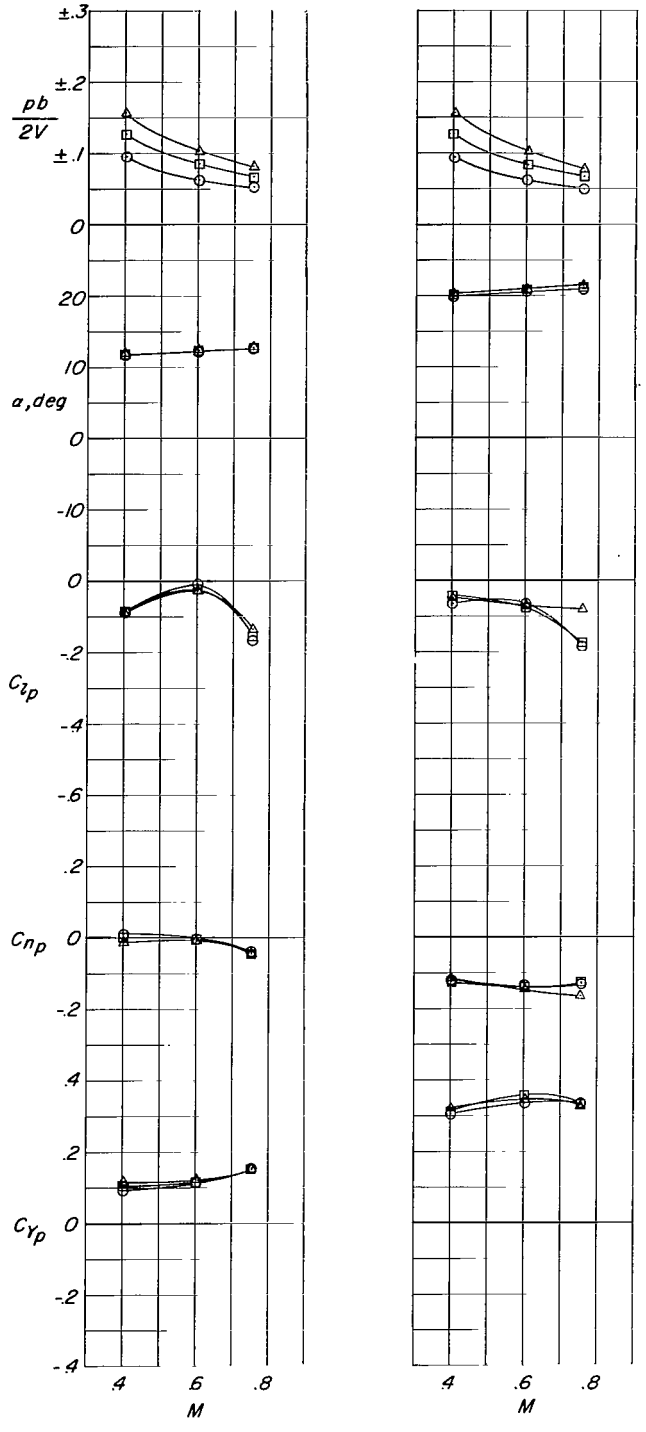

Figure 9.- Concluded.

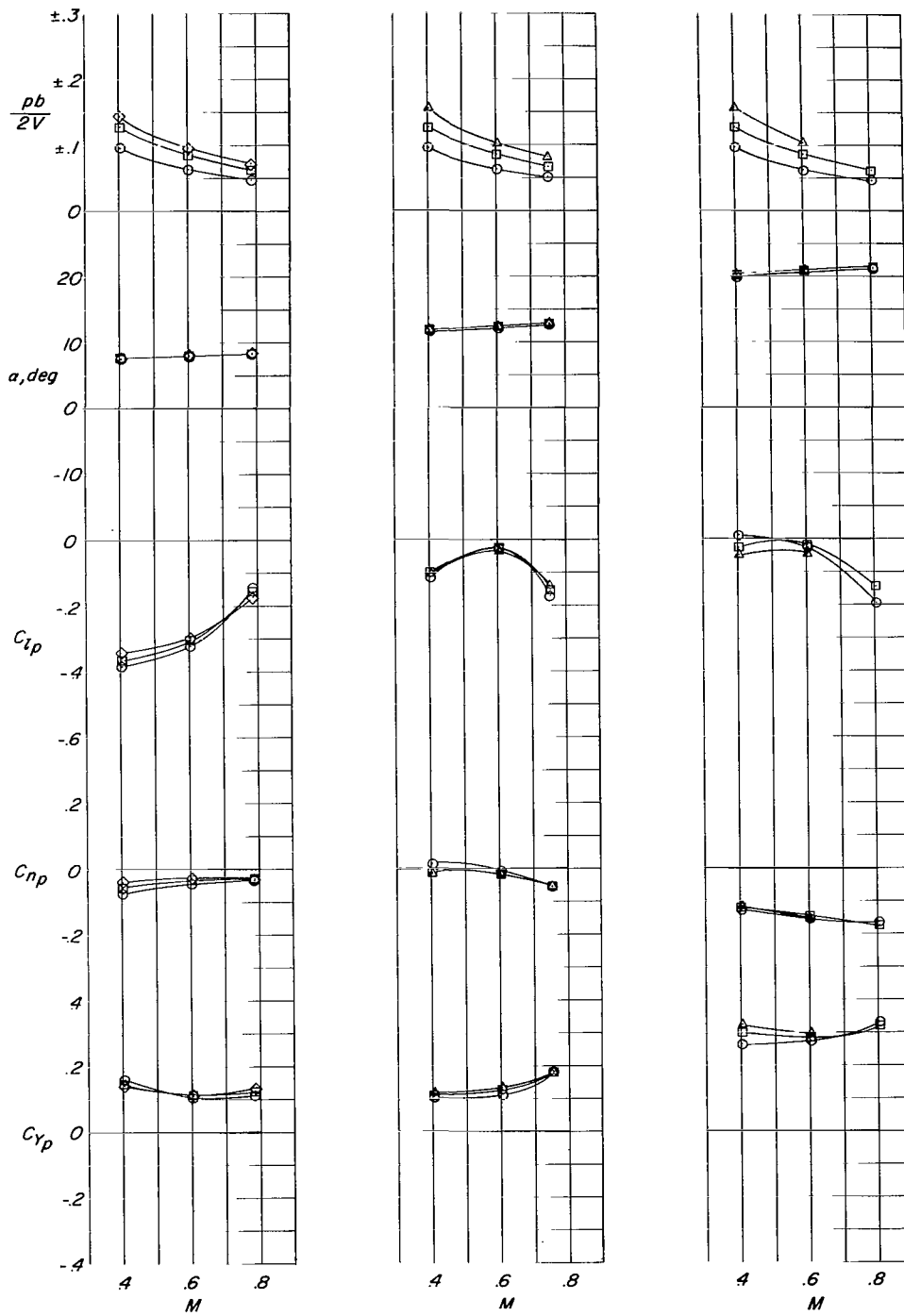

Figure 10.- Variation of rolling stability derivatives with Mach number for configuration A with $FW_{20}VH$. $i_t = -20^0$.

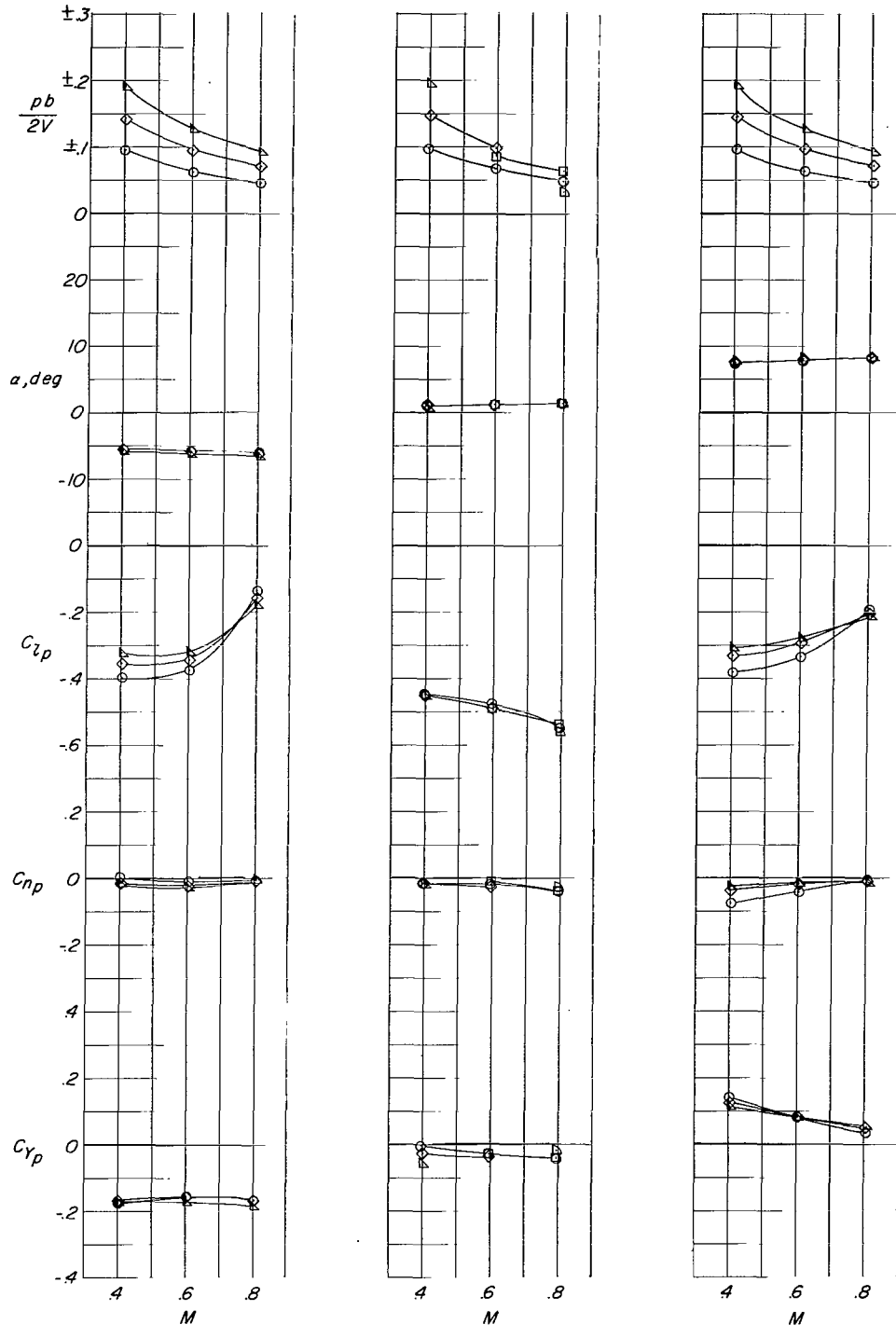

Figure 11.- Variation of rolling stability derivatives with Mach number for configuration A with $FW_{20}V$.

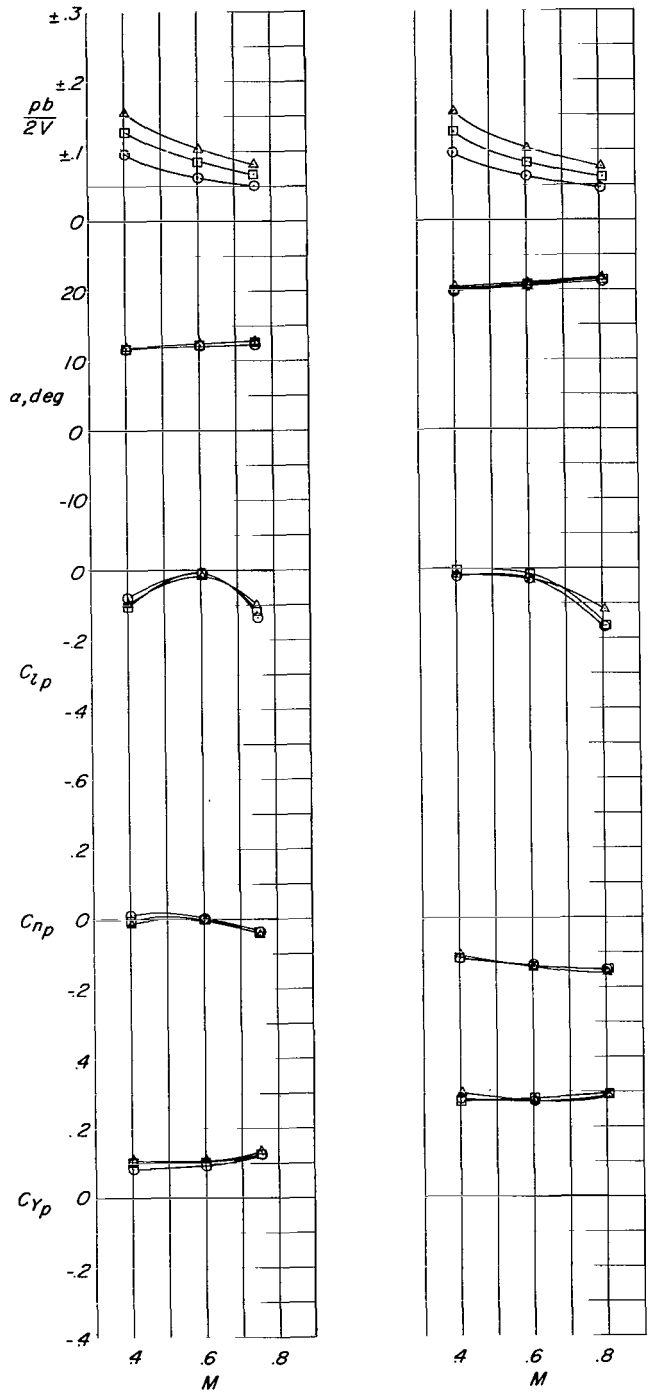

Figure 11.- Concluded.

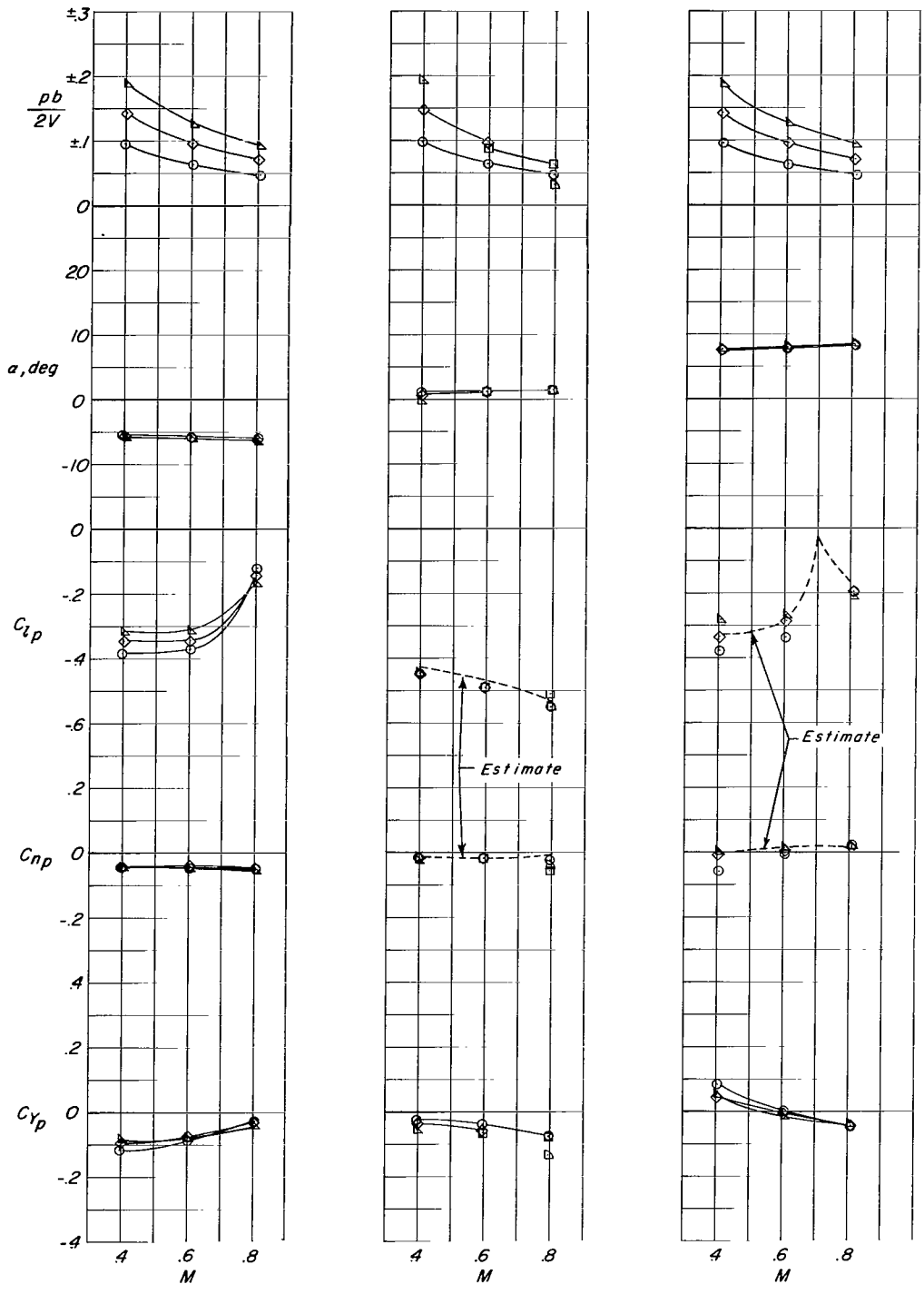

Figure 12.- Variation of rolling stability derivatives with Mach number for configuration A with FW_{20}.

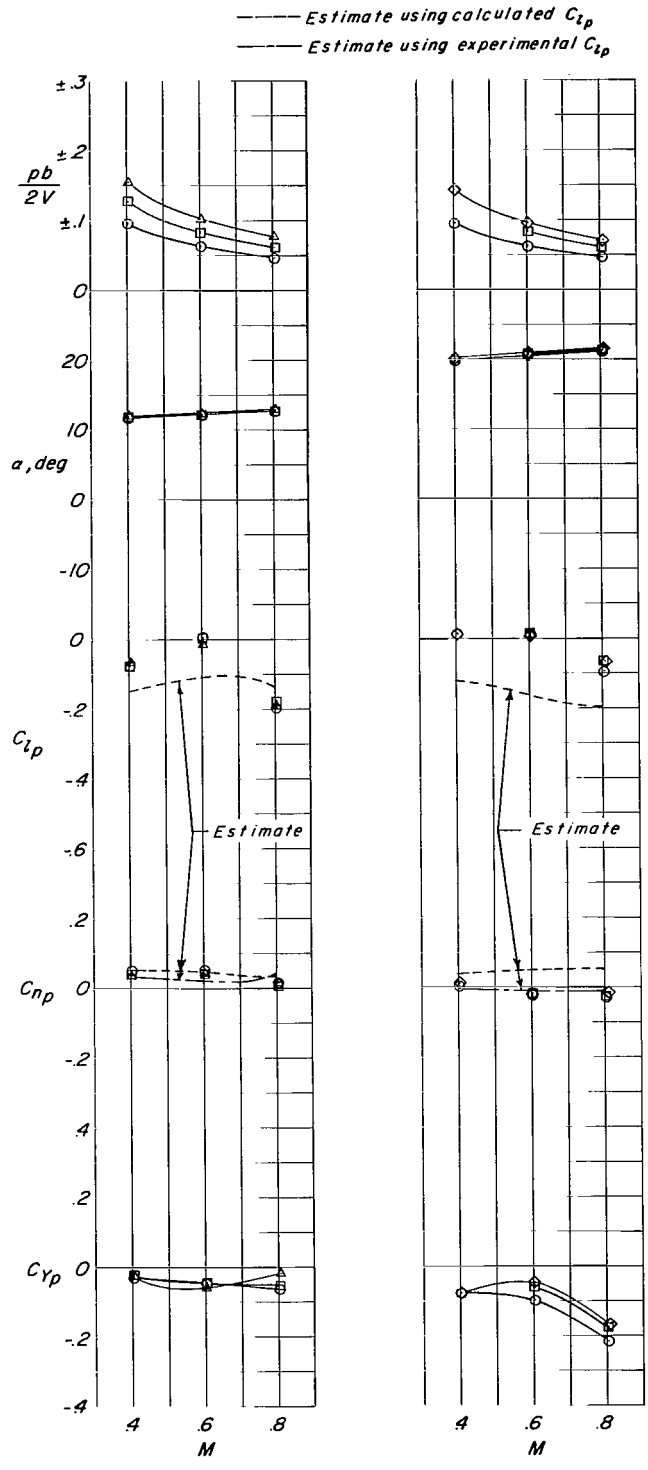

Figure 12.- Concluded.

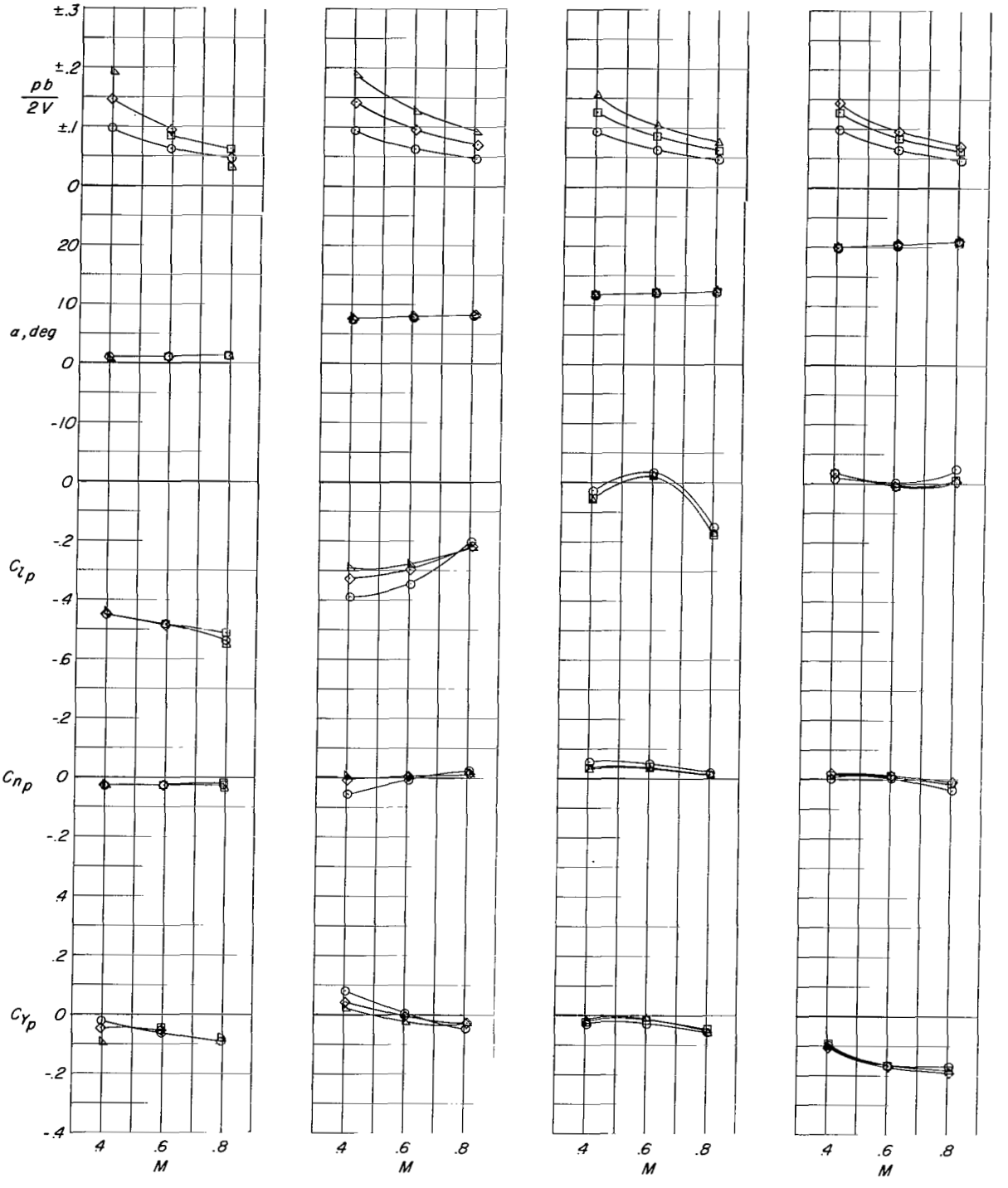

Figure 13.- Variation of rolling stability derivatives with Mach number for configuration A with FW_{20} and glove off.

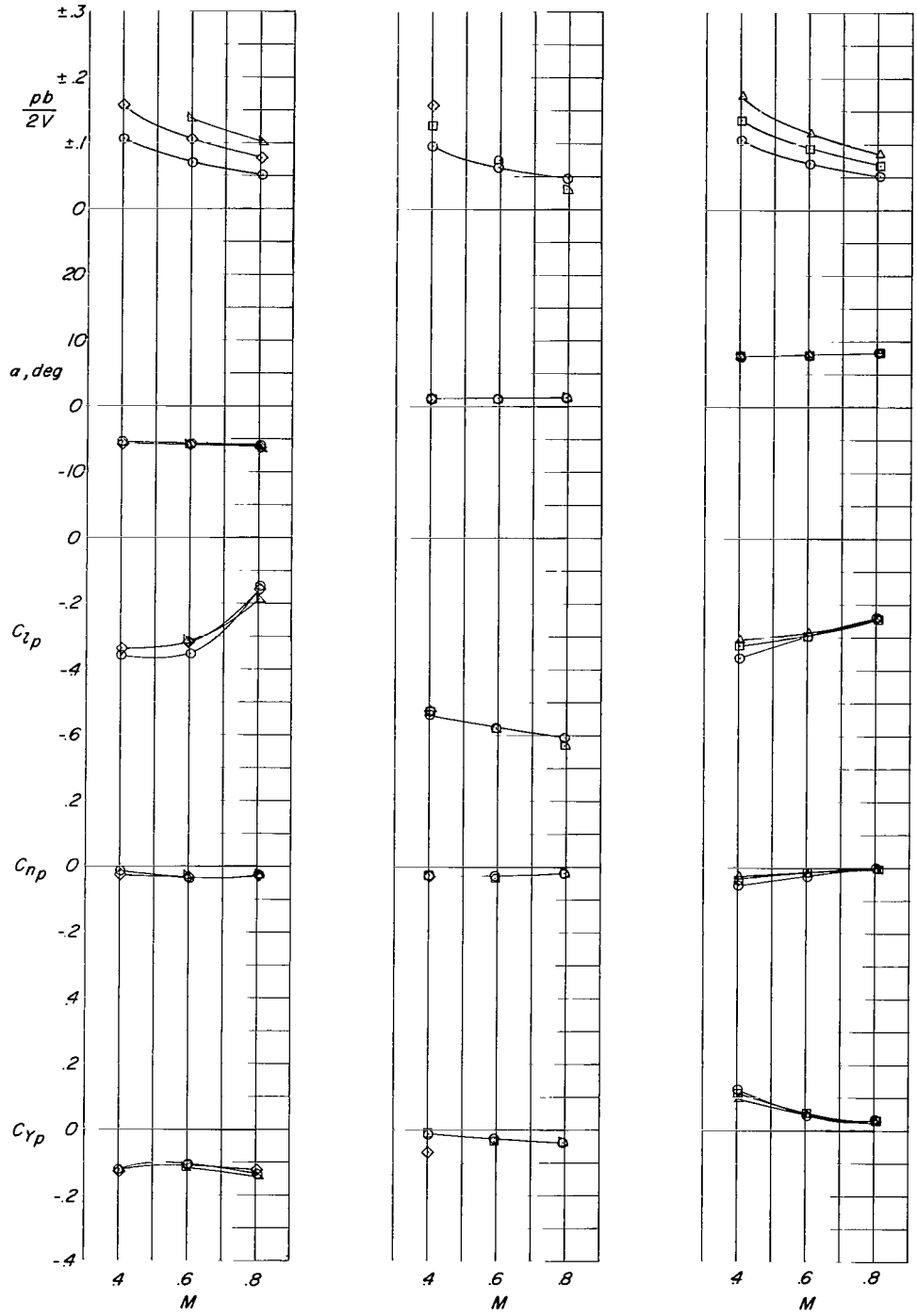

Figure 14.- Variation of rolling stability derivatives with Mach number for configuration B with $FW_{20}VH$. $i_t = 0^o$.

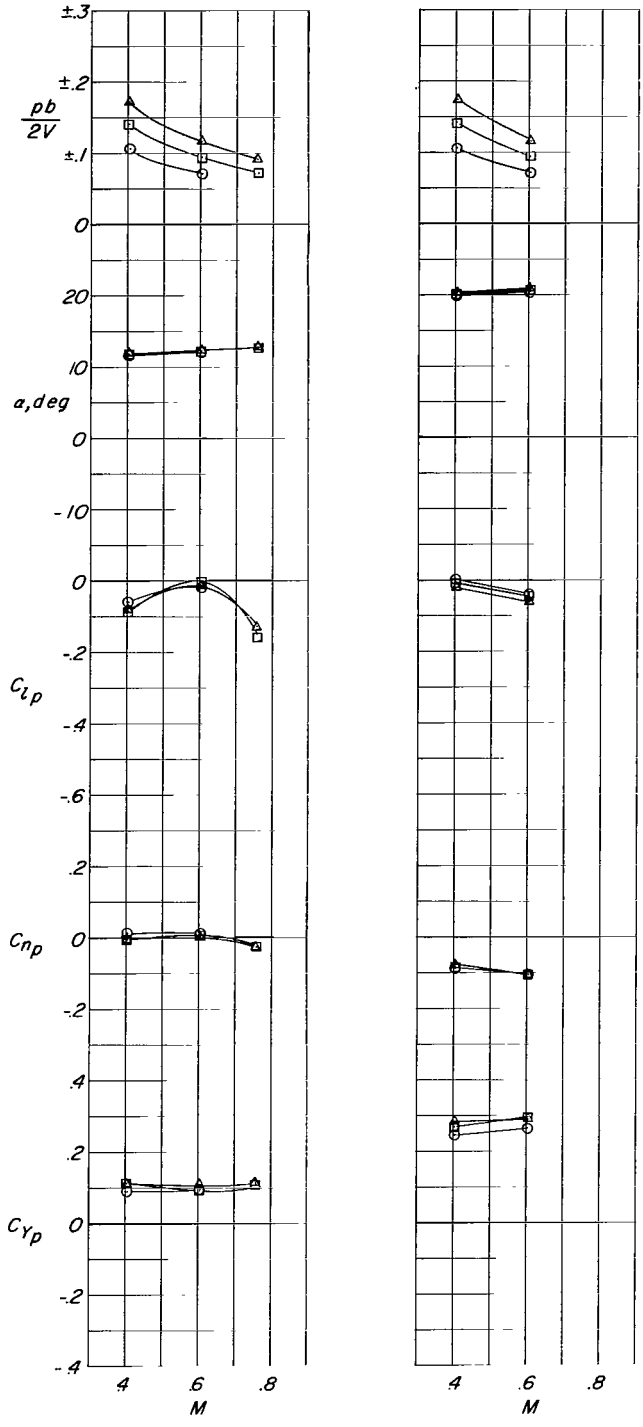

Figure 14.- Concluded.

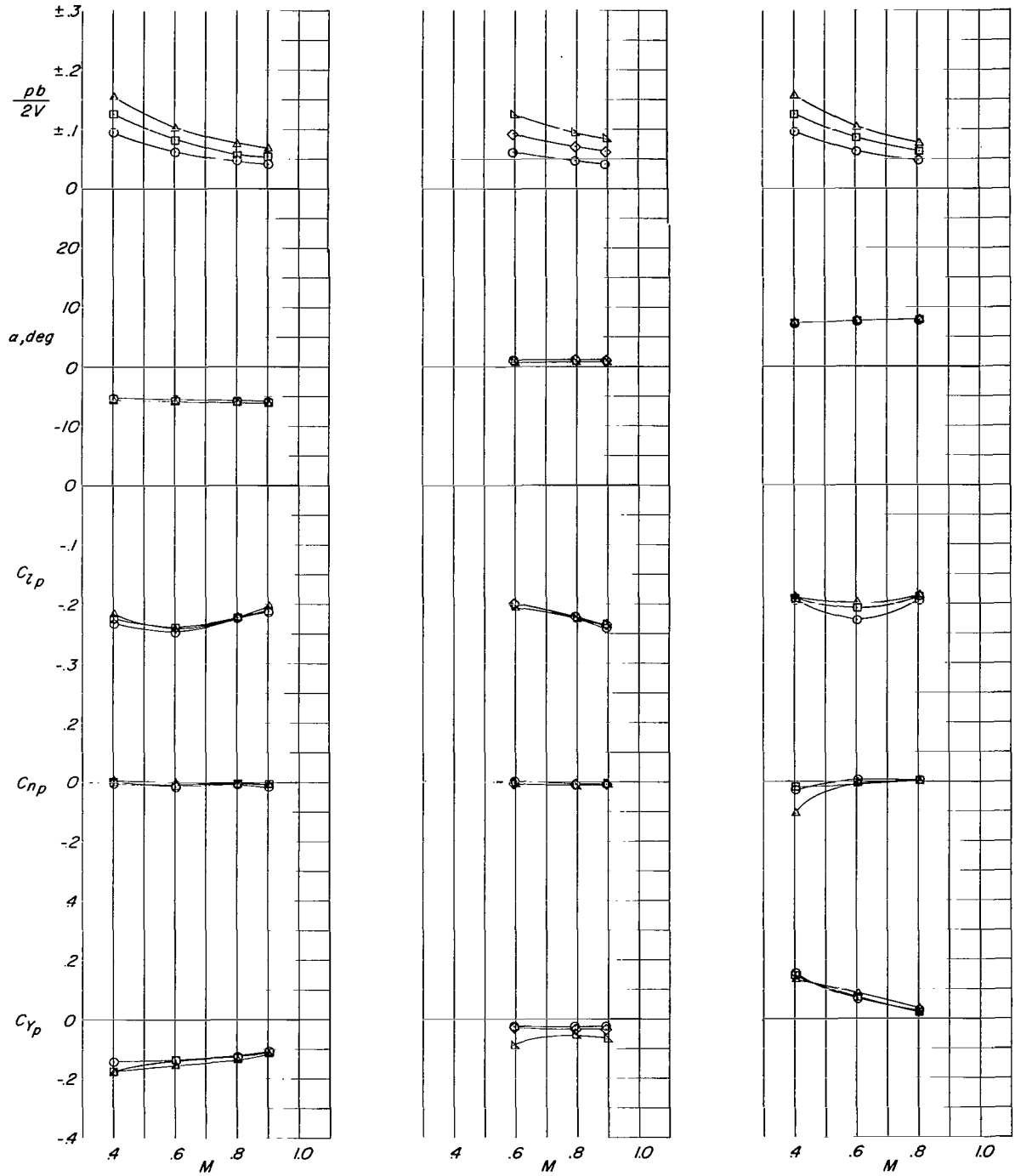

Figure 15.- Variation of rolling stability derivatives with Mach number for configuration A with $FW_{50}VH$. $i_t = 0^0$.

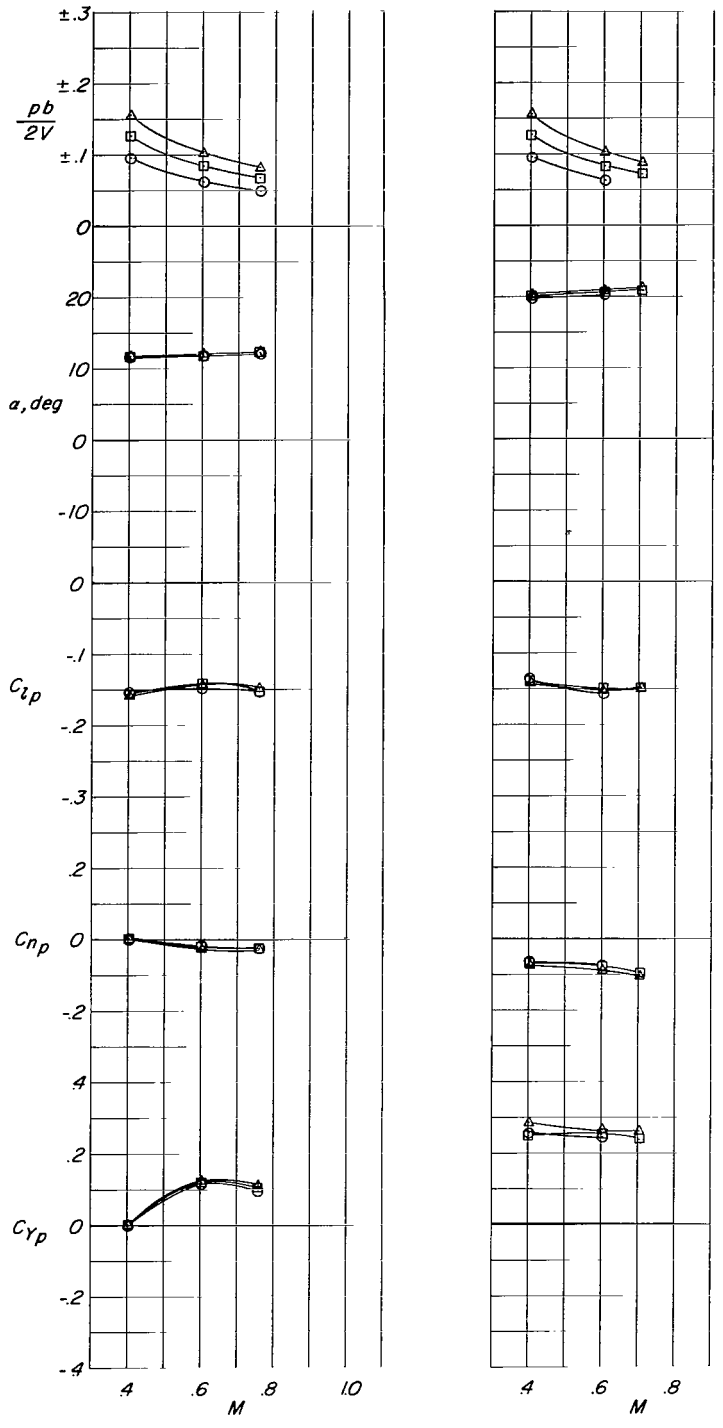

Figure 15.- Concluded.

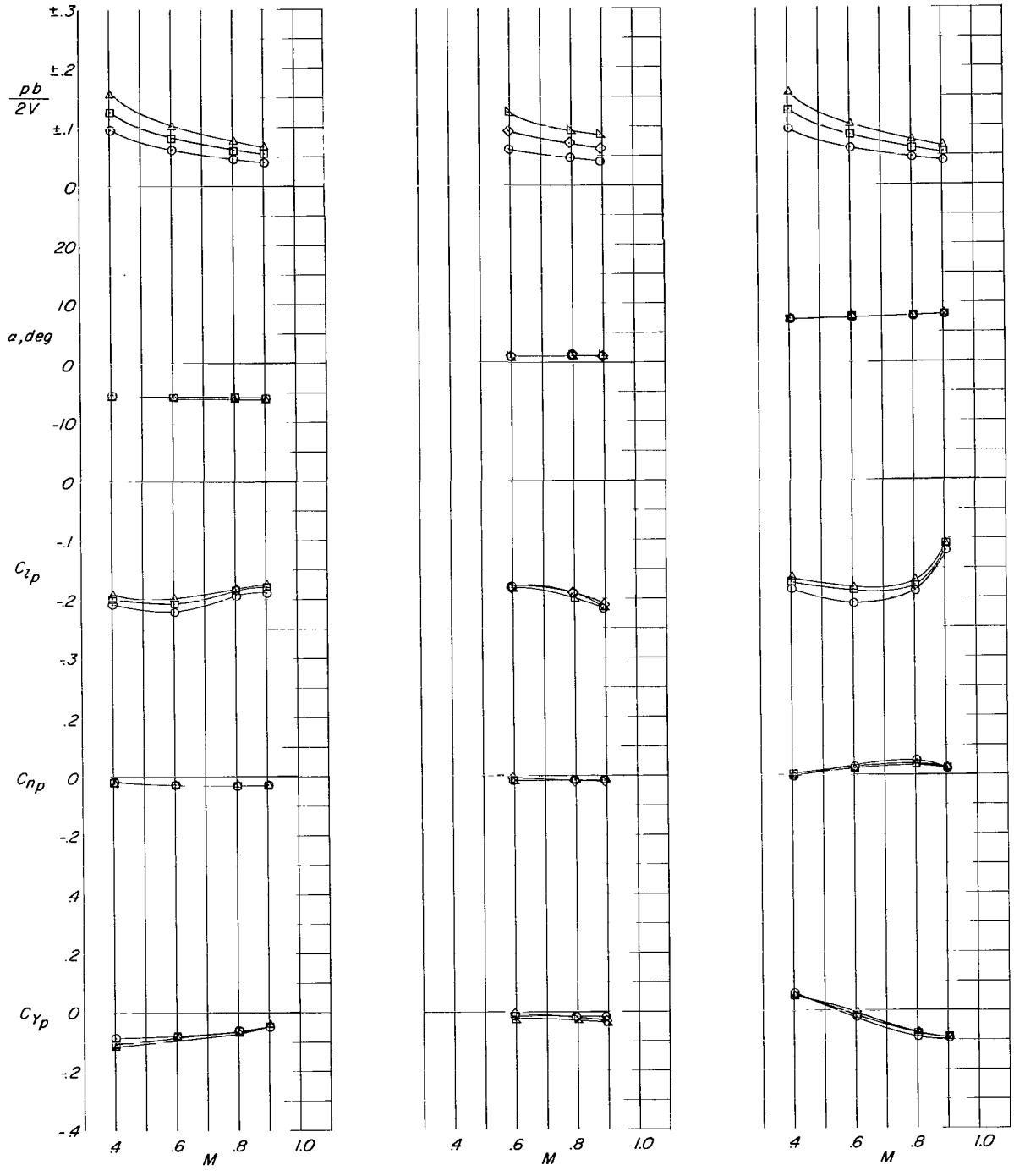

Figure 16.- Variation of rolling stability derivatives with Mach number for configuration A with FW_{50}.

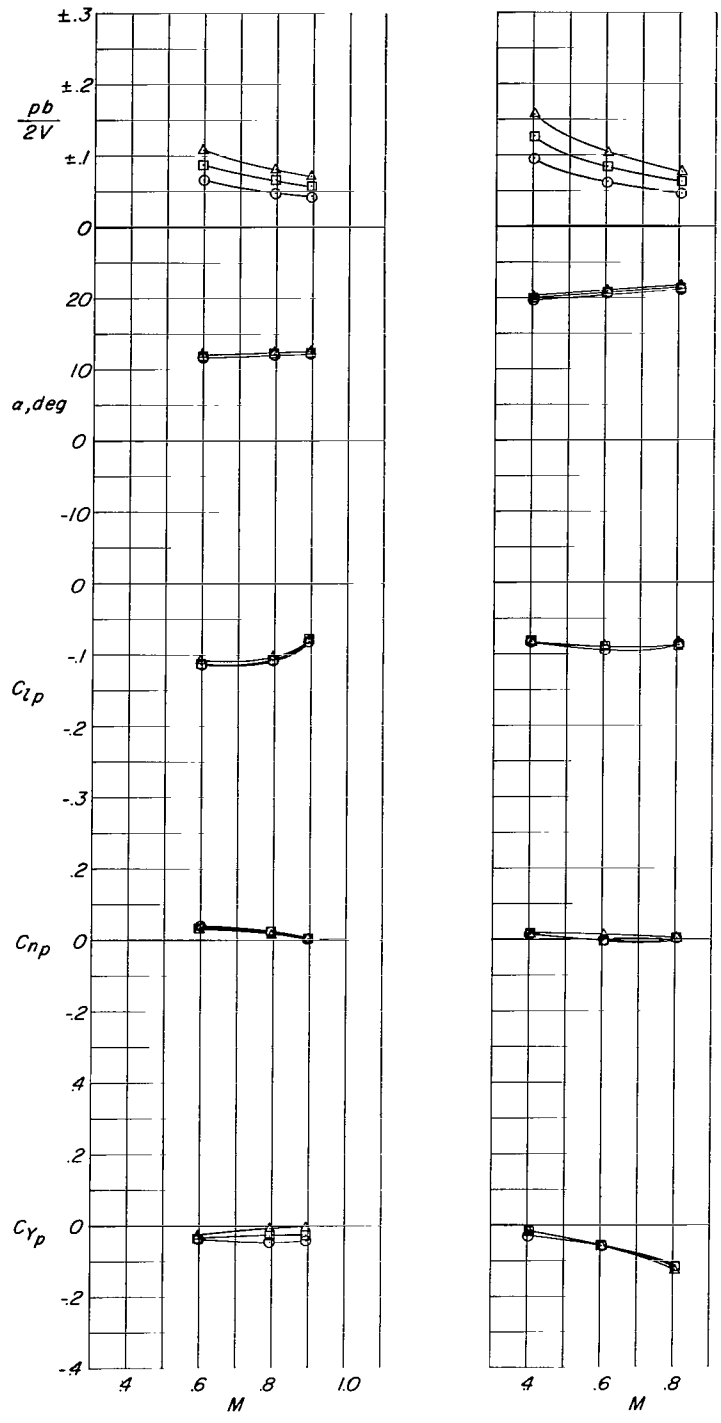

Figure 16.- Concluded.

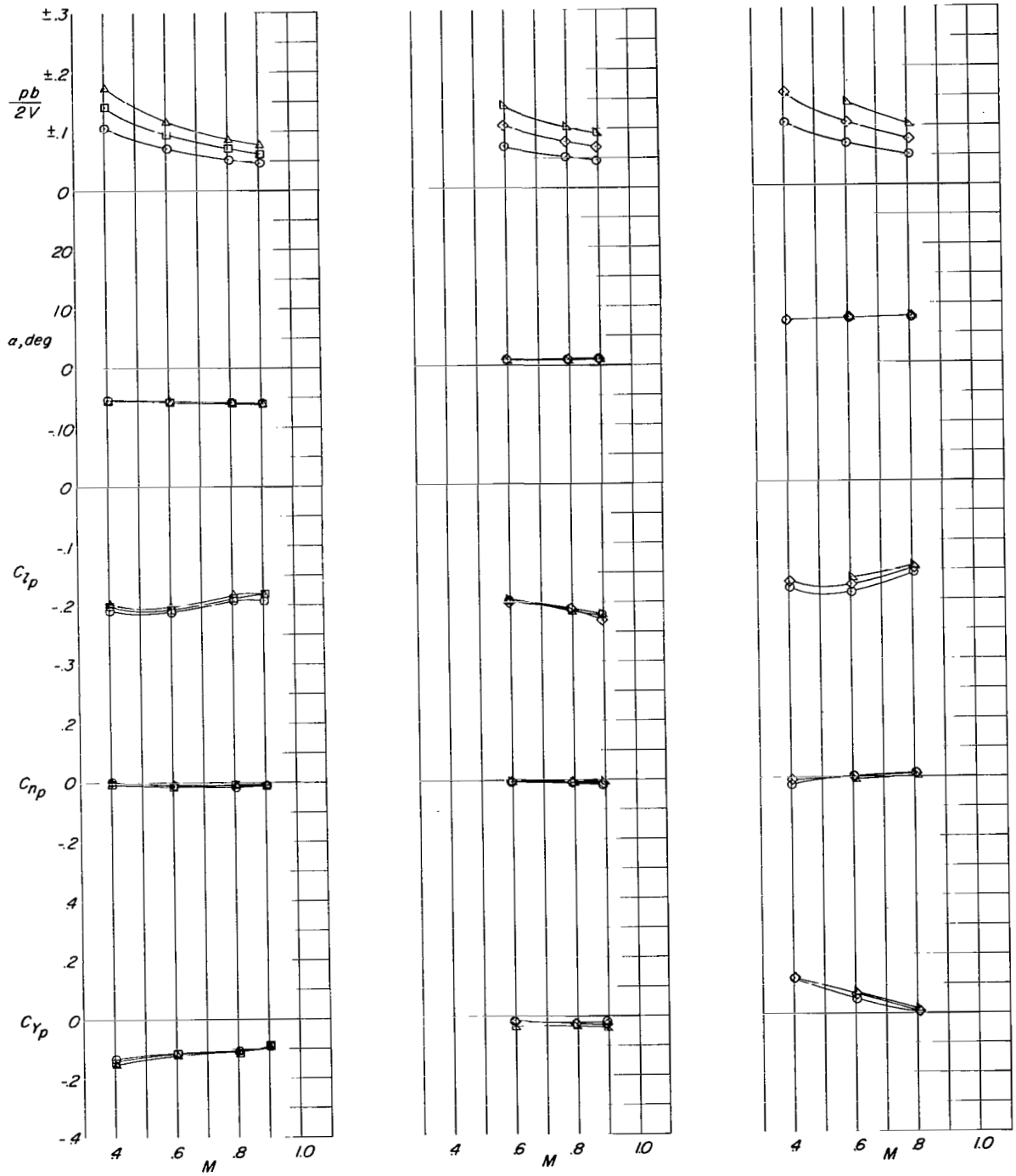

Figure 17.- Variation of rolling stability derivatives with Mach number for configuration B with $FW_{50}VH$. $i_t = 0^0$.

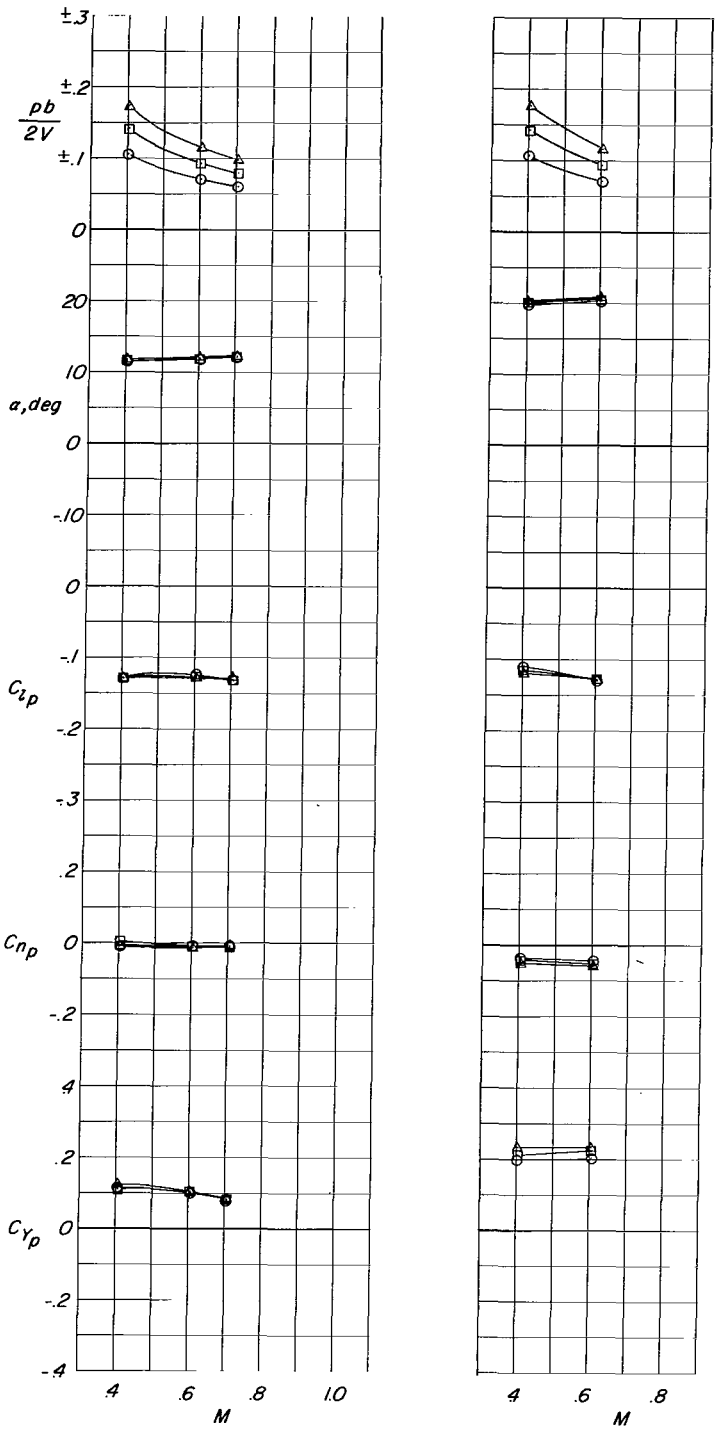

Figure 17.- Concluded.

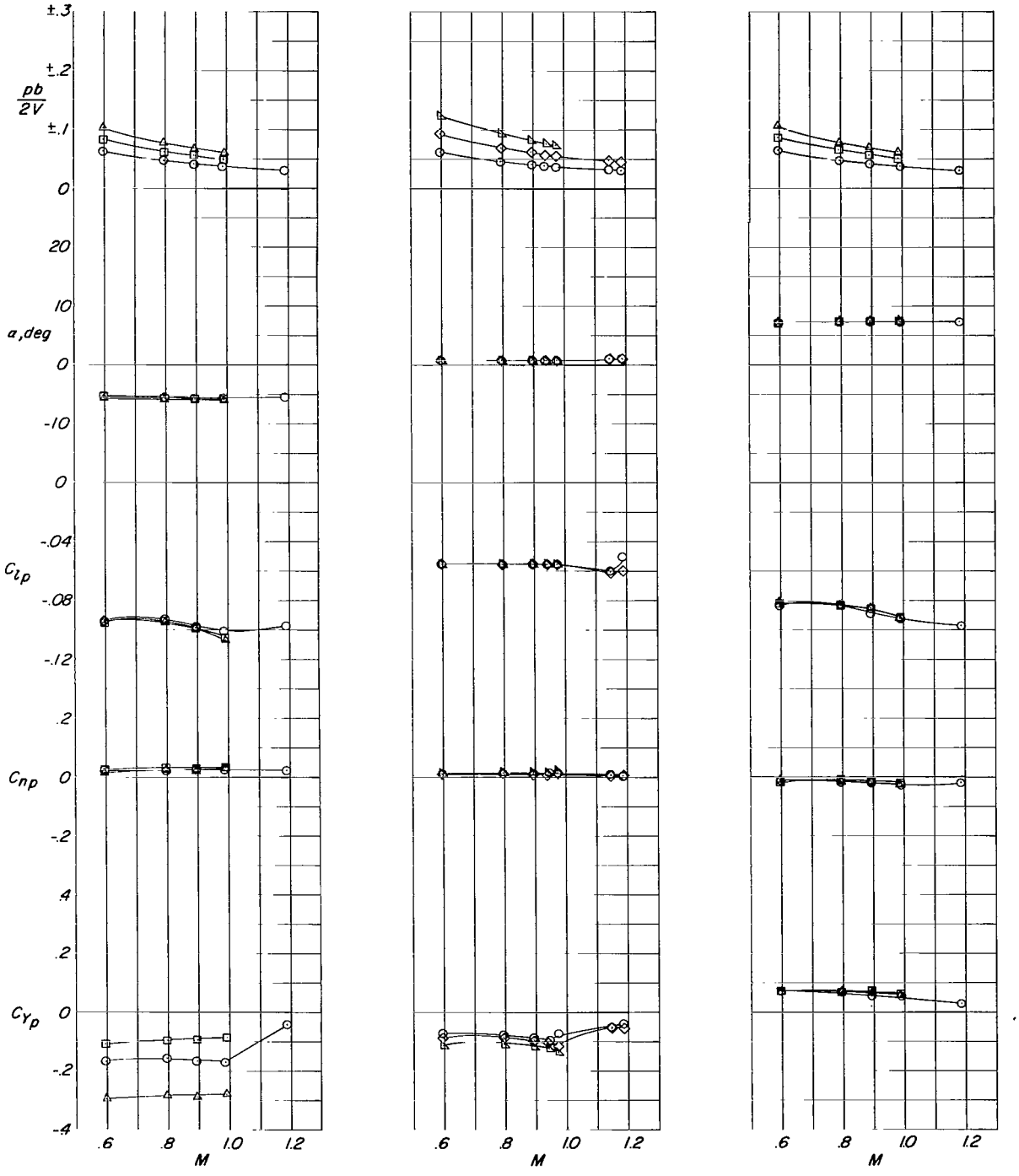

Figure 18.- Variation of rolling stability derivatives with Mach number for configuration A with $FW_{72.5}VH$. $i_t = 0^0$.

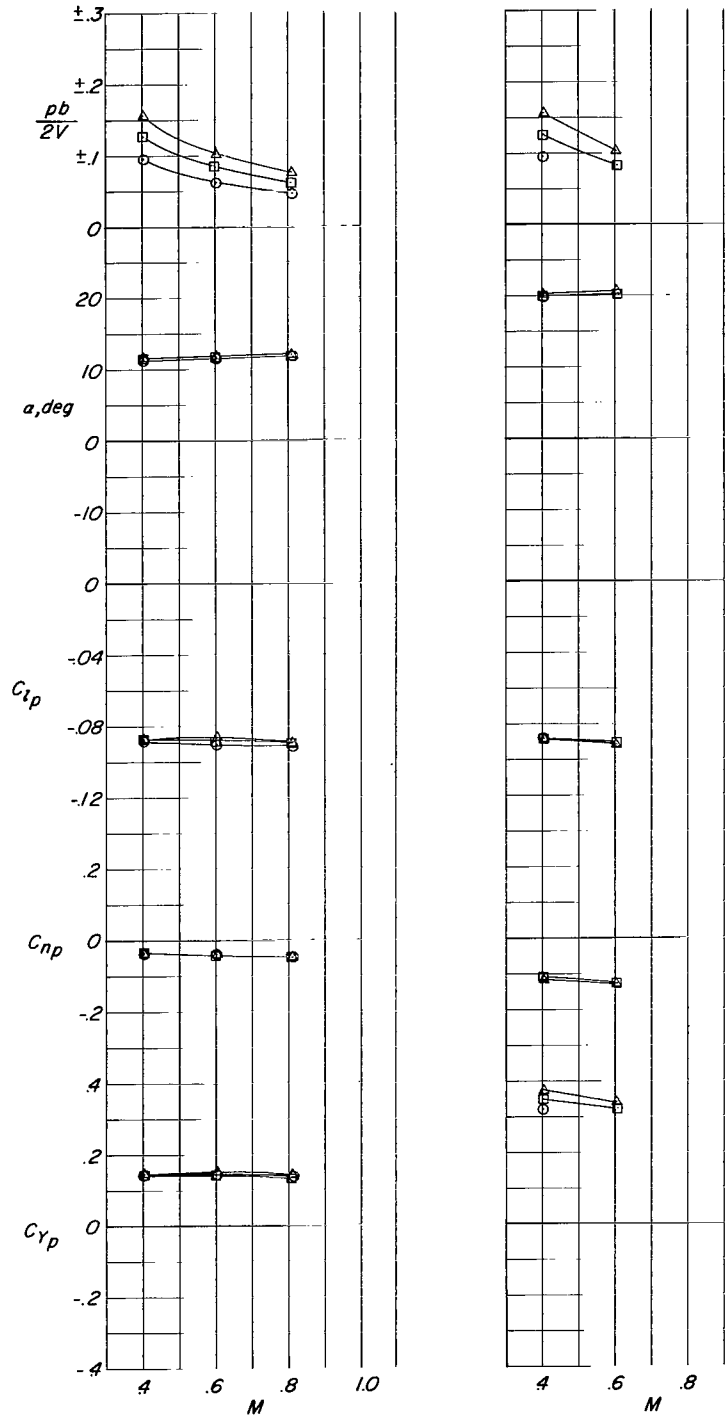

Figure 18.- Concluded.

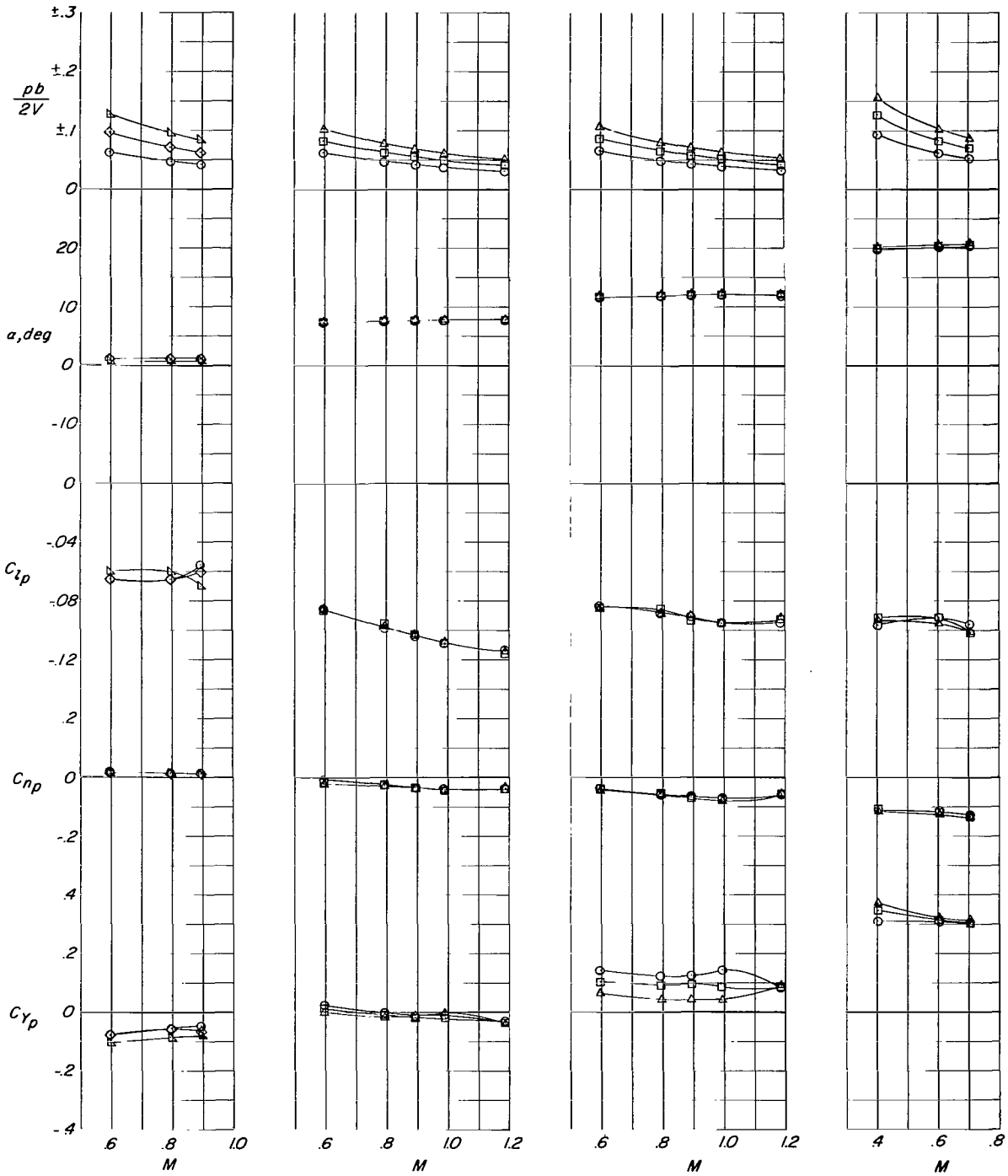

Figure 19.- Variation of rolling stability derivatives with Mach number for configuration A with $FW_{72.5}VH$. $i_t = -10^0$.

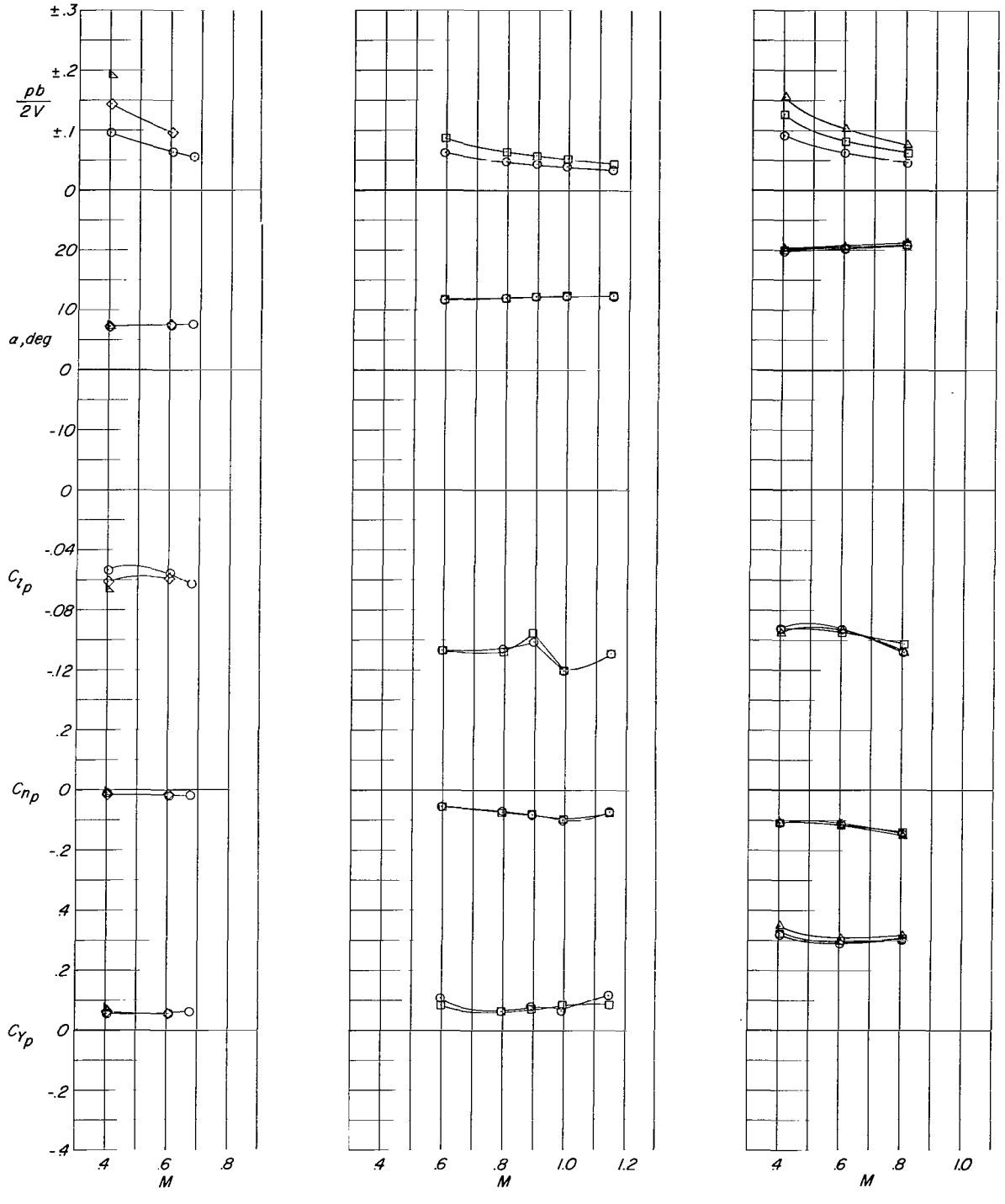

Figure 20.- Variation of rolling stability derivatives with Mach number for configuration A with $FW_{72.5}VH$. $i_t = -20^0$.

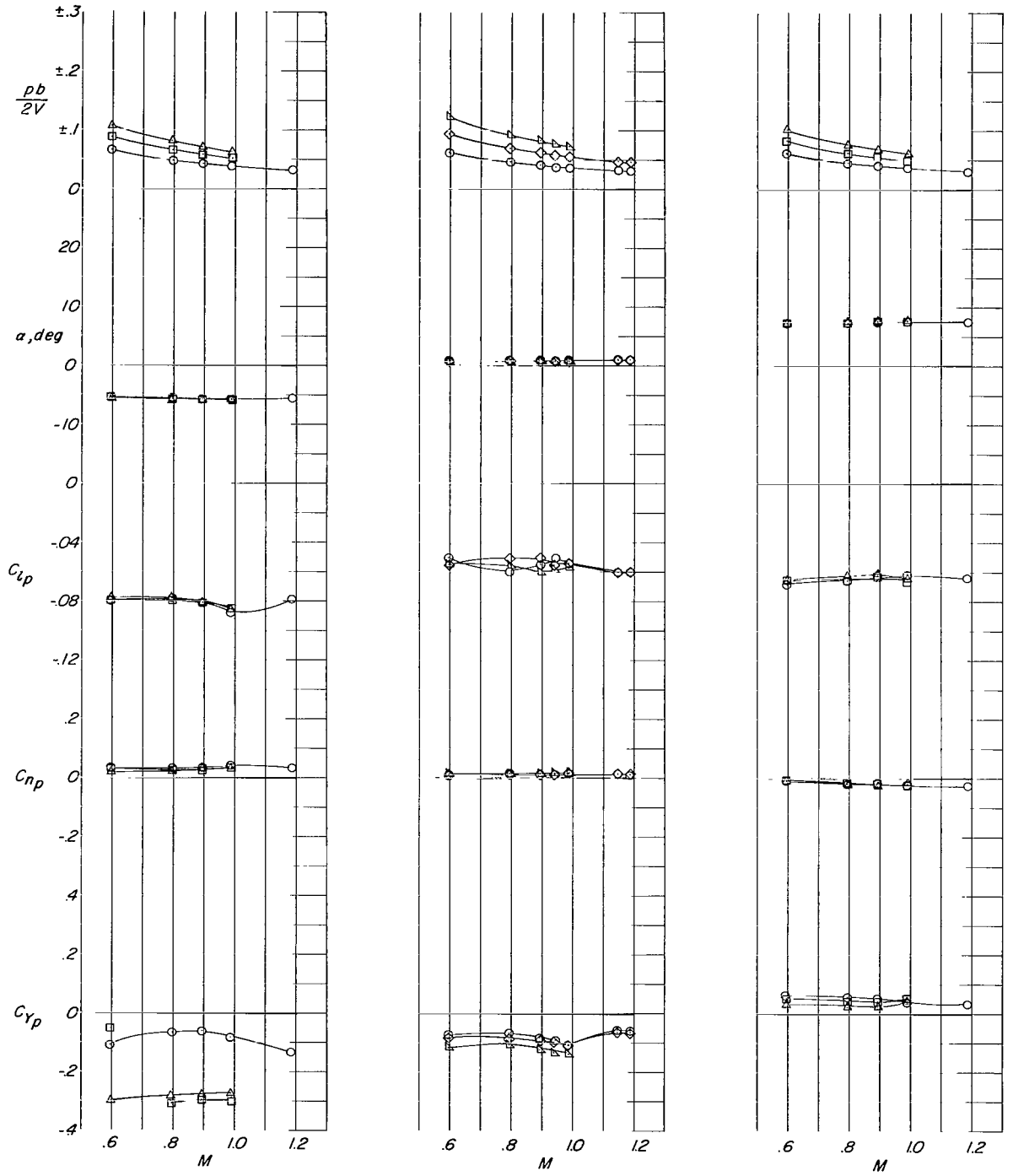

Figure 21.- Variation of rolling stability derivatives with Mach number for configuration A with $FW_{72.5}V$.

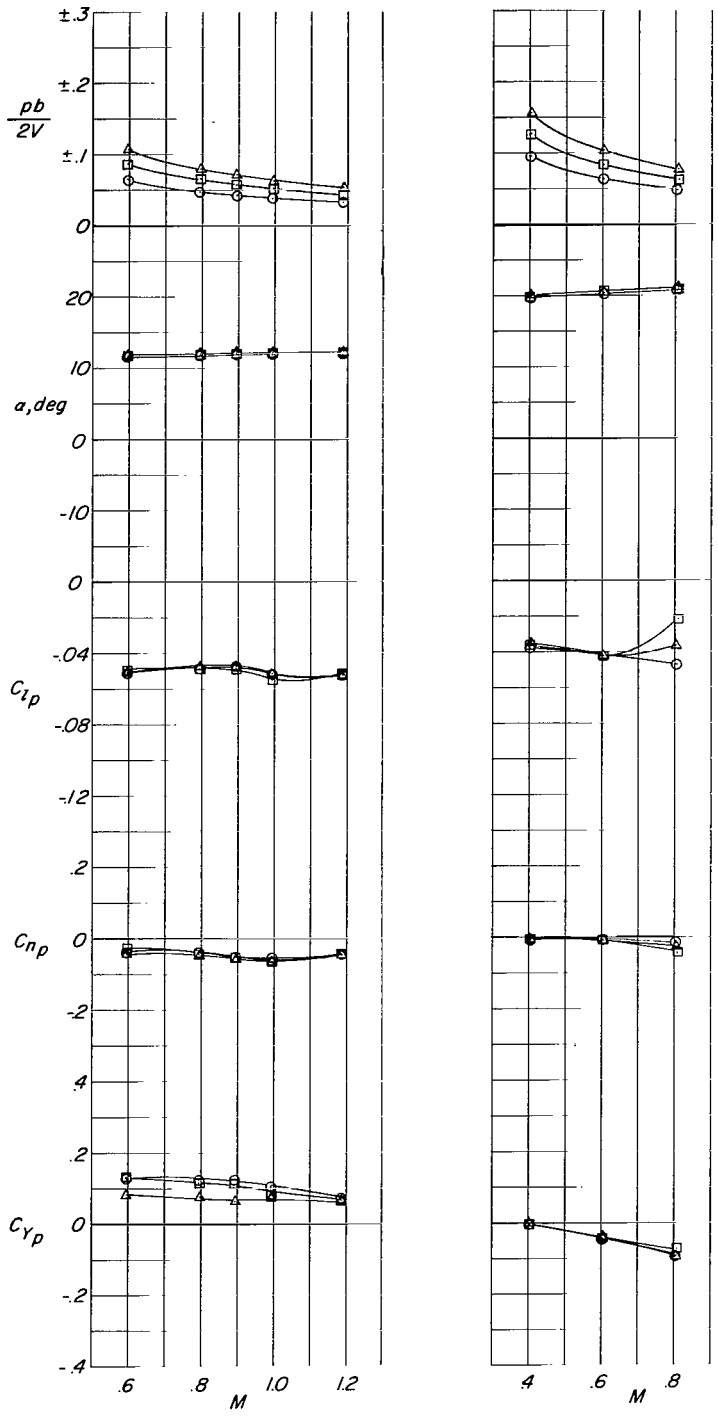

Figure 21.- Concluded.

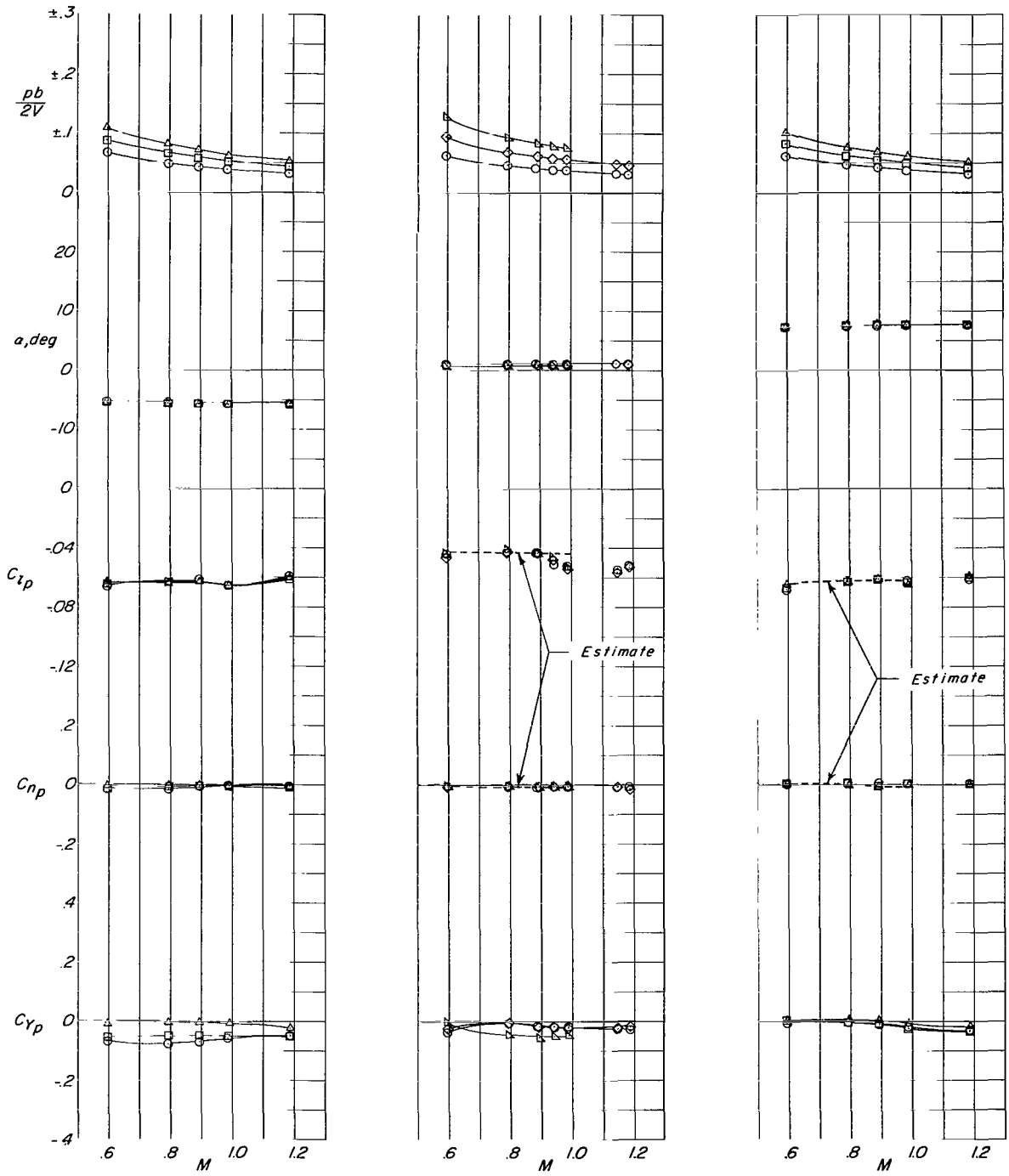

Figure 22.- Variation of rolling stability derivatives with Mach number for configuration A with $FW_{72.5}$.

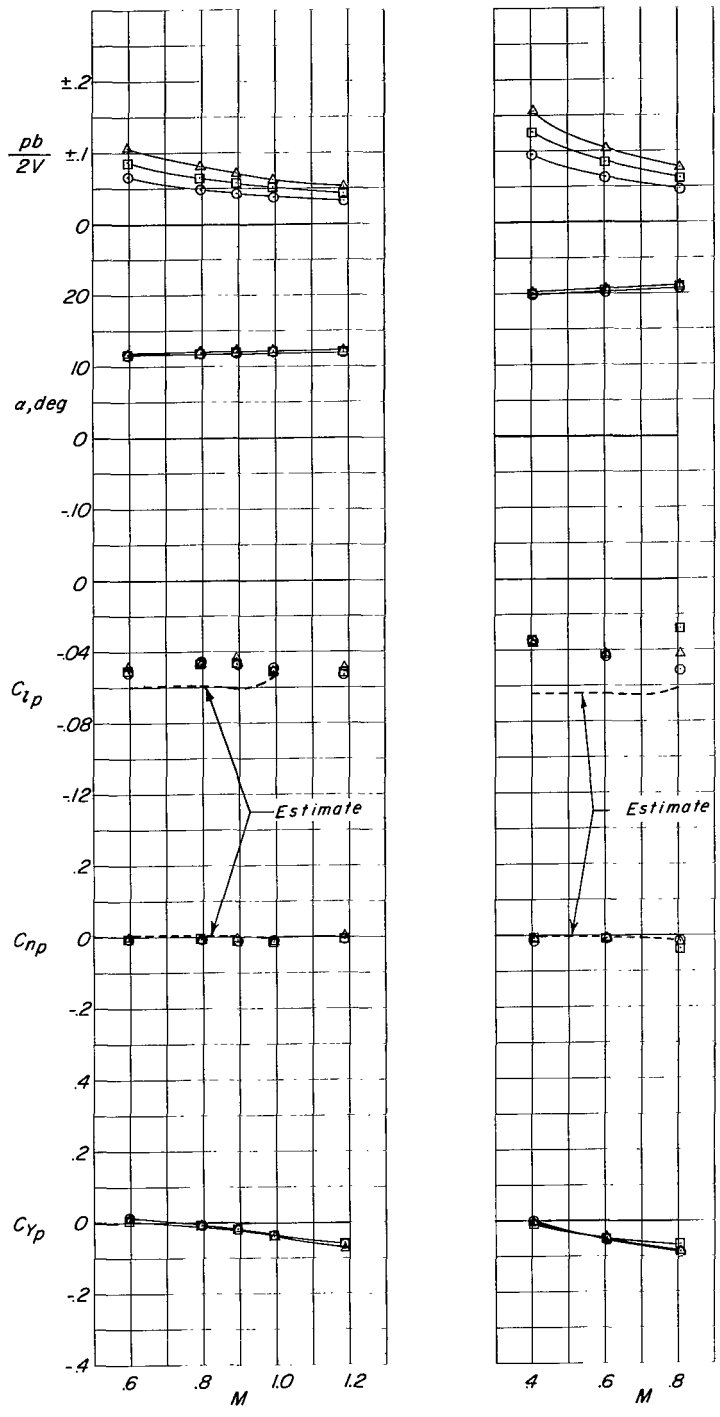

Figure 22.- Concluded.

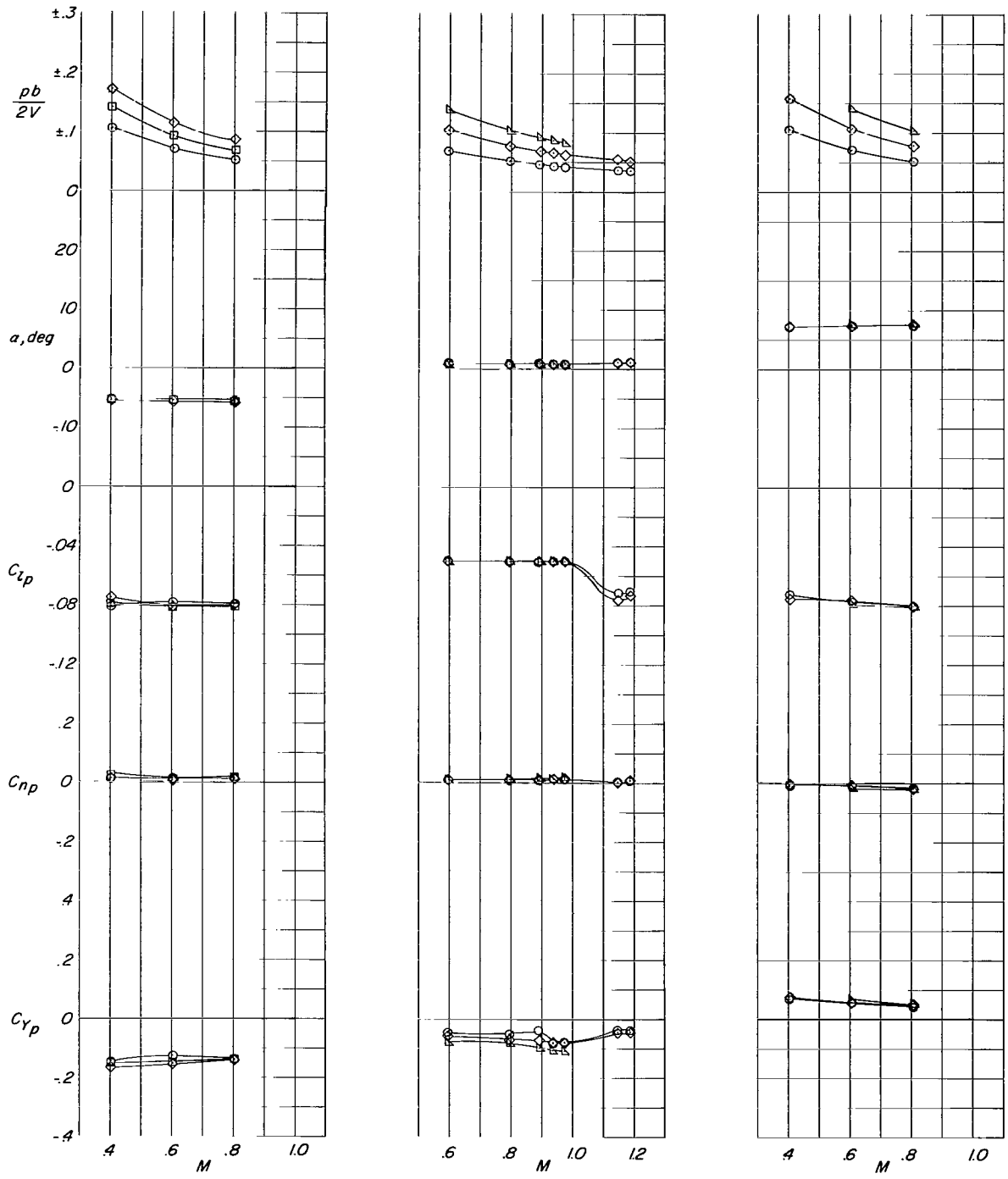

Figure 23.- Variation of rolling stability derivatives with Mach number for configuration B with $FW_{72.5}VH$. $i_t = 0^0$.

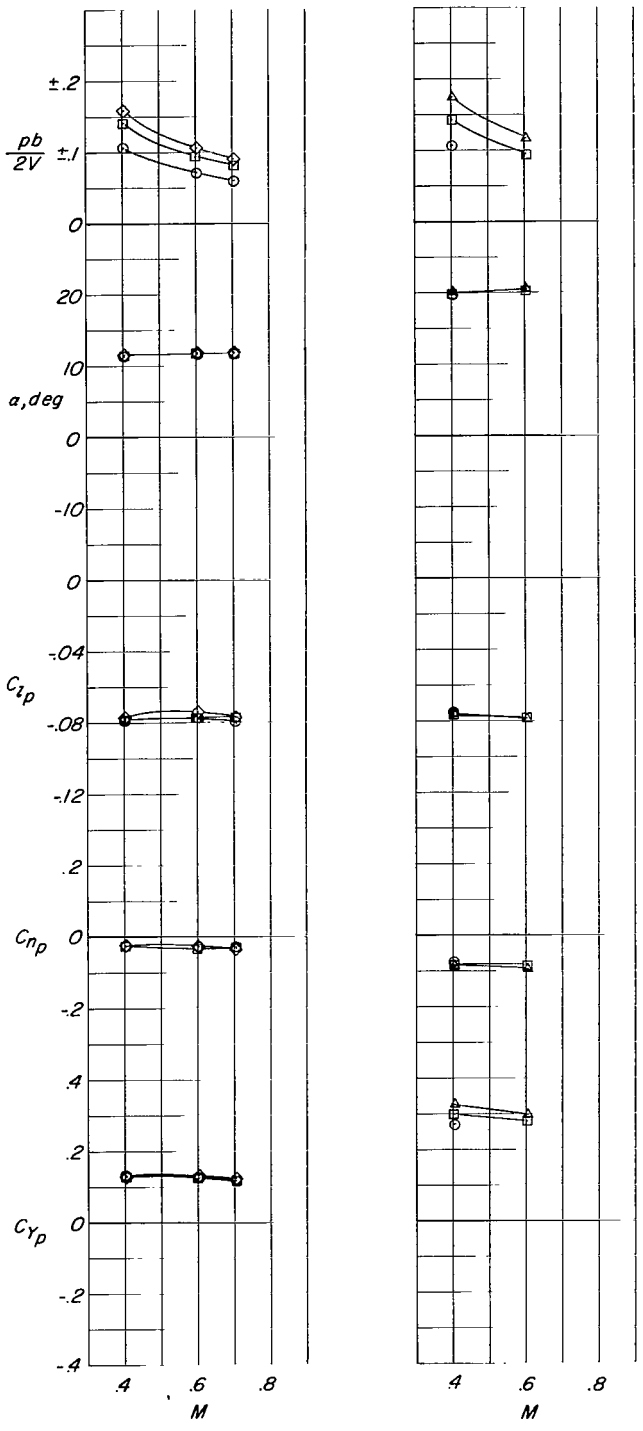

Figure 23.- Concluded.

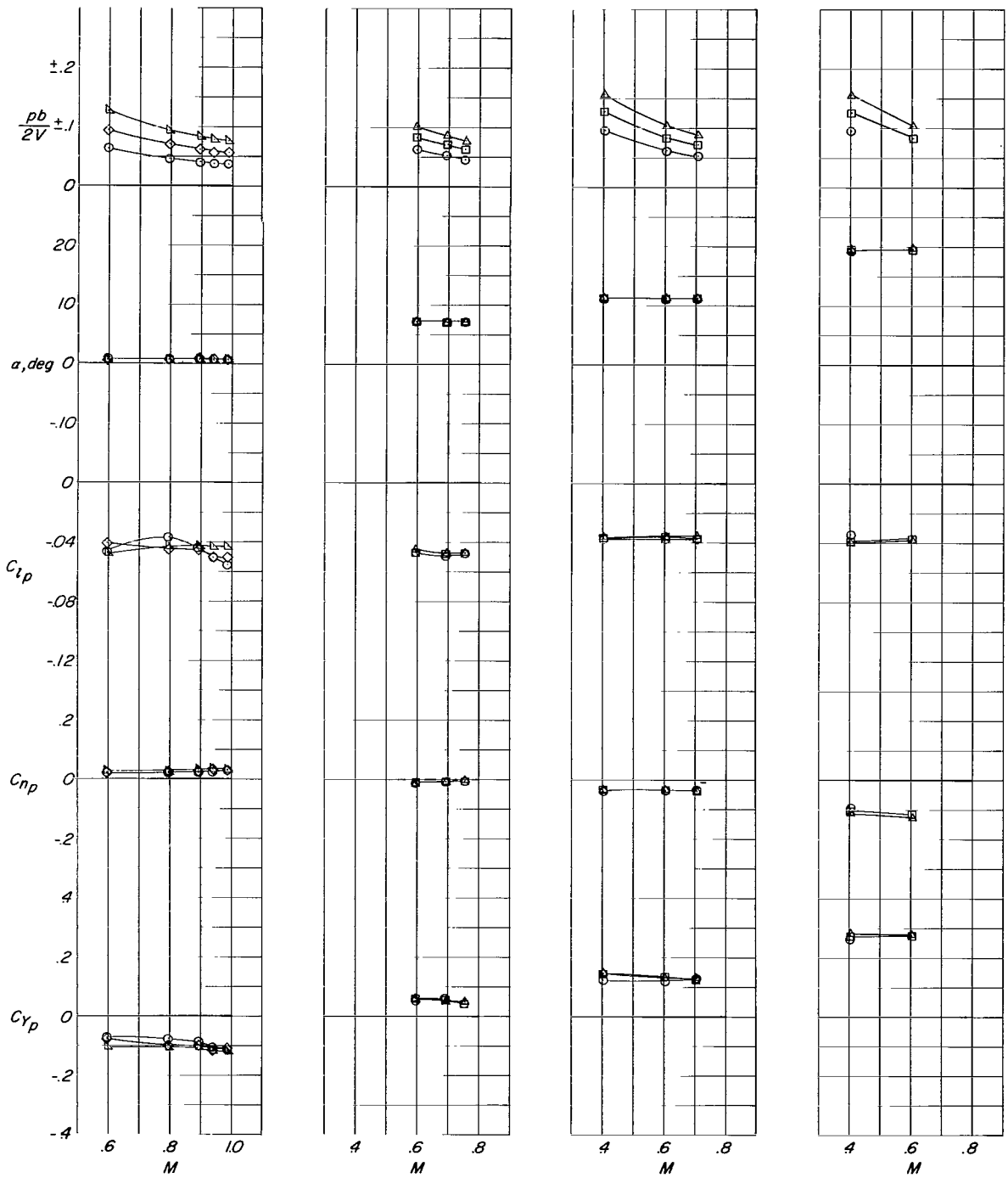

Figure 24.- Variation of rolling stability derivatives with Mach number for configuration A with FVH. $i_t = 0^o$.

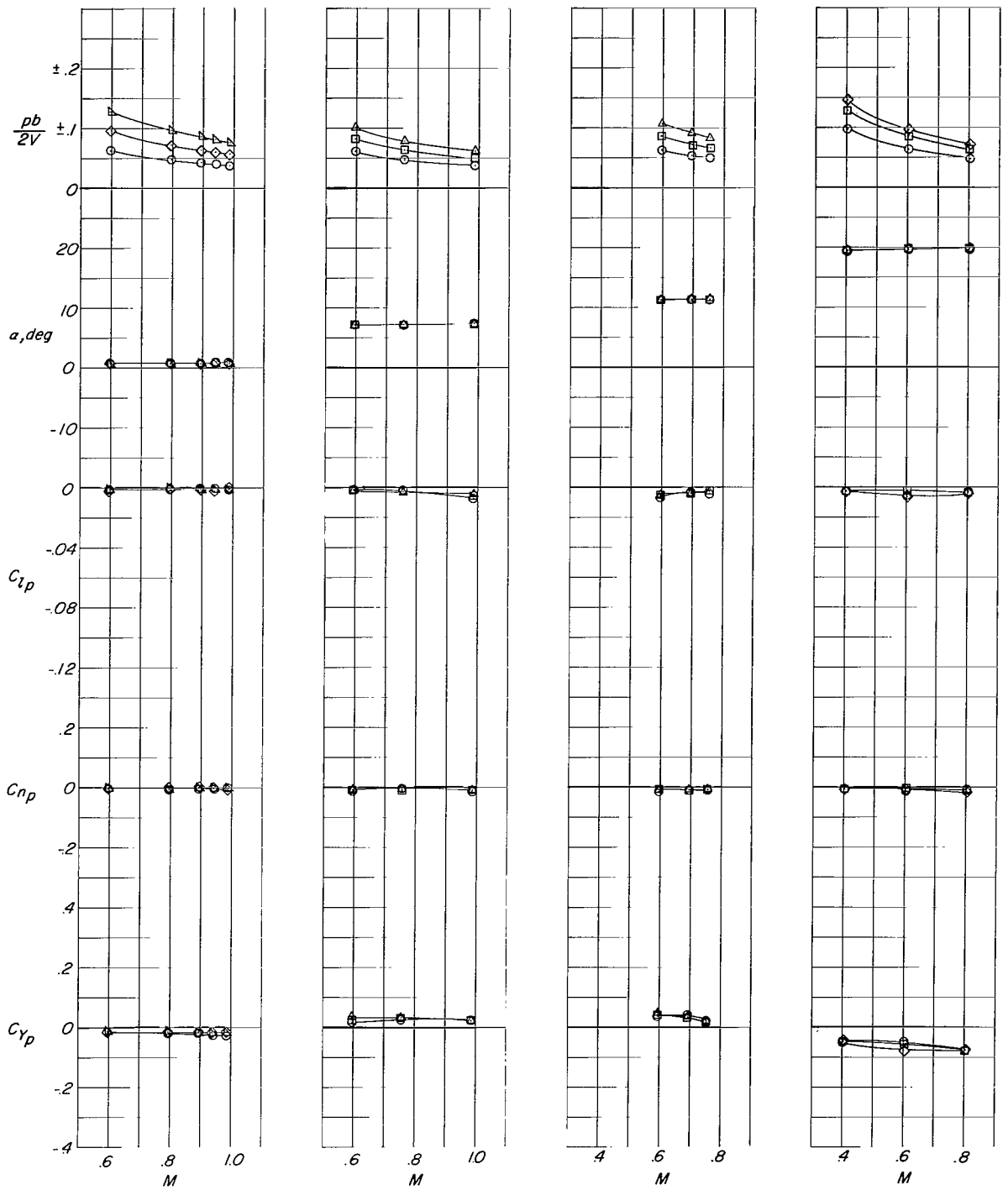

Figure 25.- Variation of rolling stability derivatives with Mach number for configuration A with F alone.

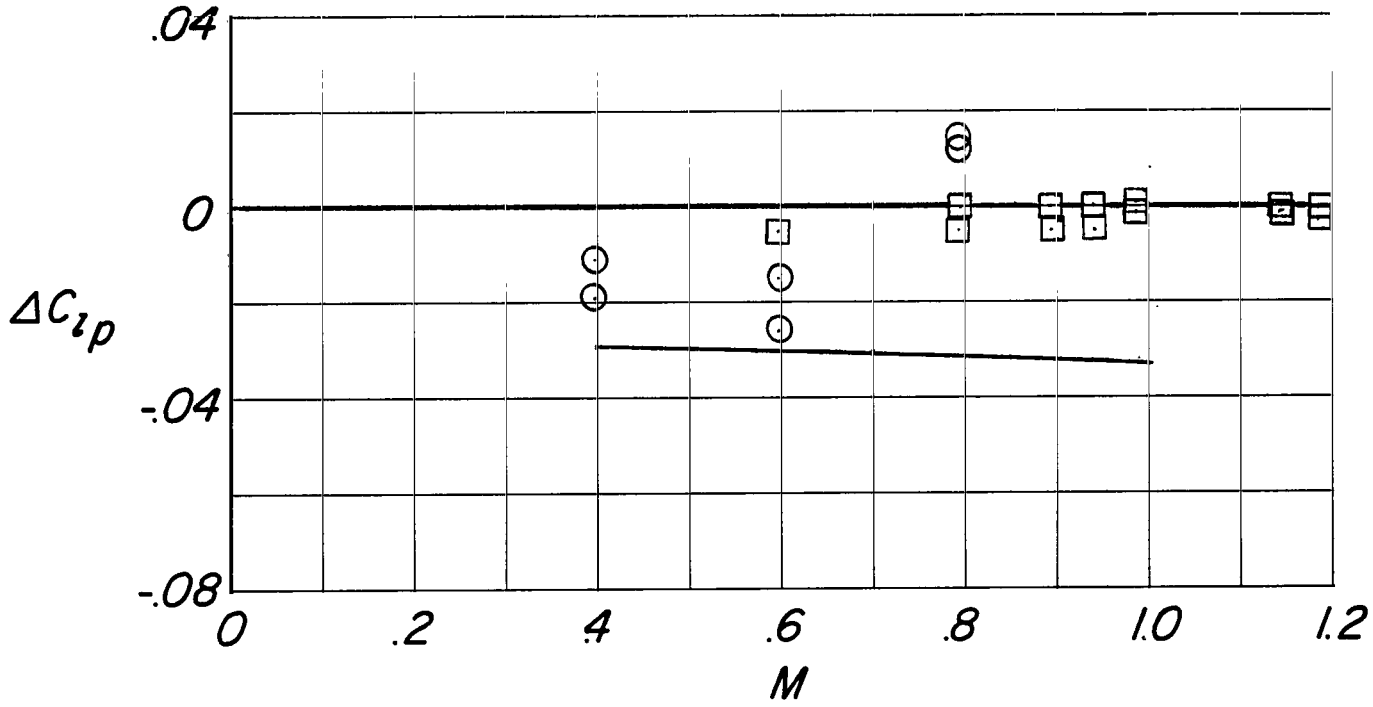

Figure 26.- Contribution of horizontal tails to C_{l_p}. $\alpha \approx 1.0^0$.

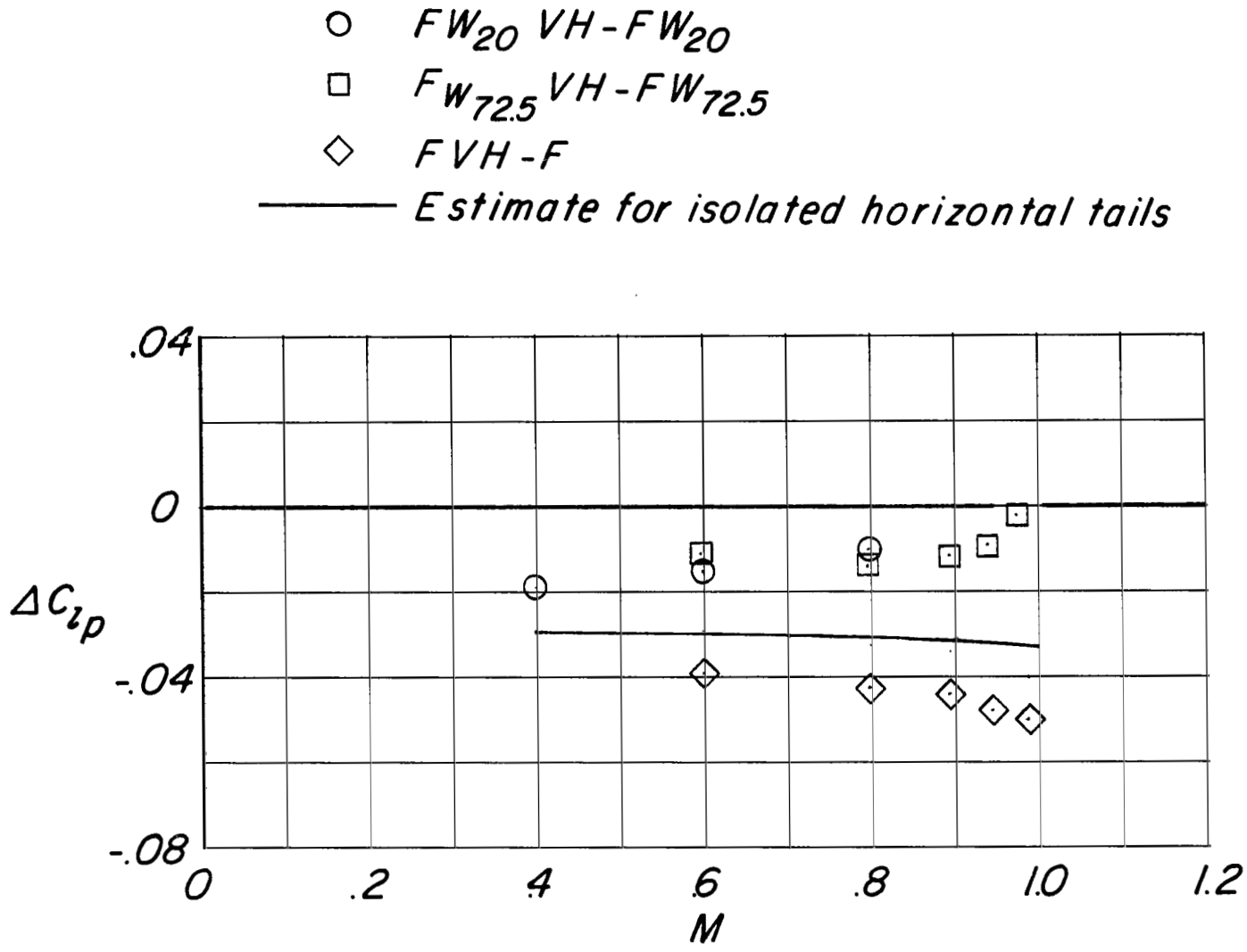

Figure 27.- Contribution of vertical and horizontal tails to C_{l_p}. $\alpha \approx 1.0^{0}$.

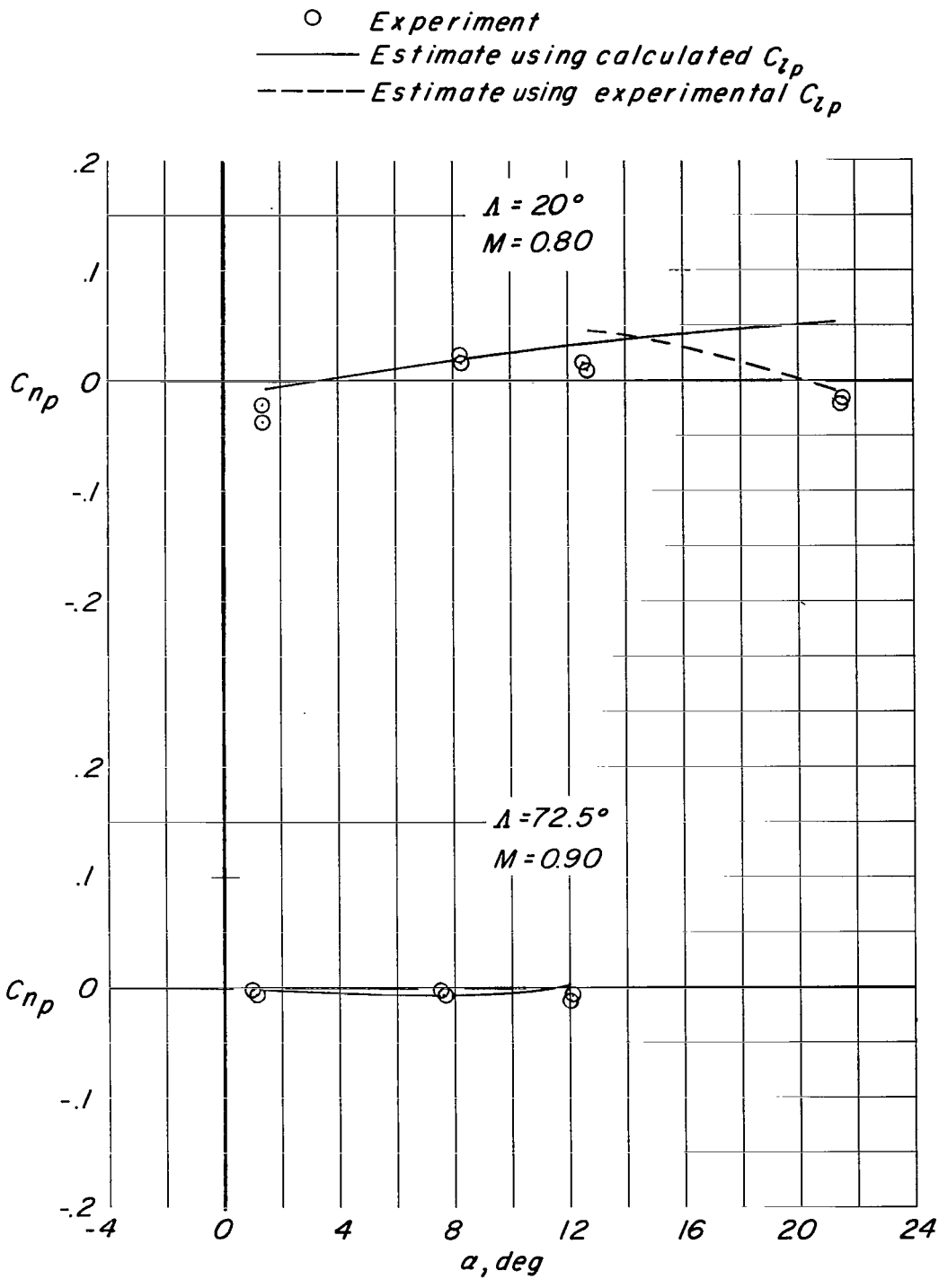

Figure 28.- Comparison of experimental and estimated C_{n_p} for wing-fuselage combinations.

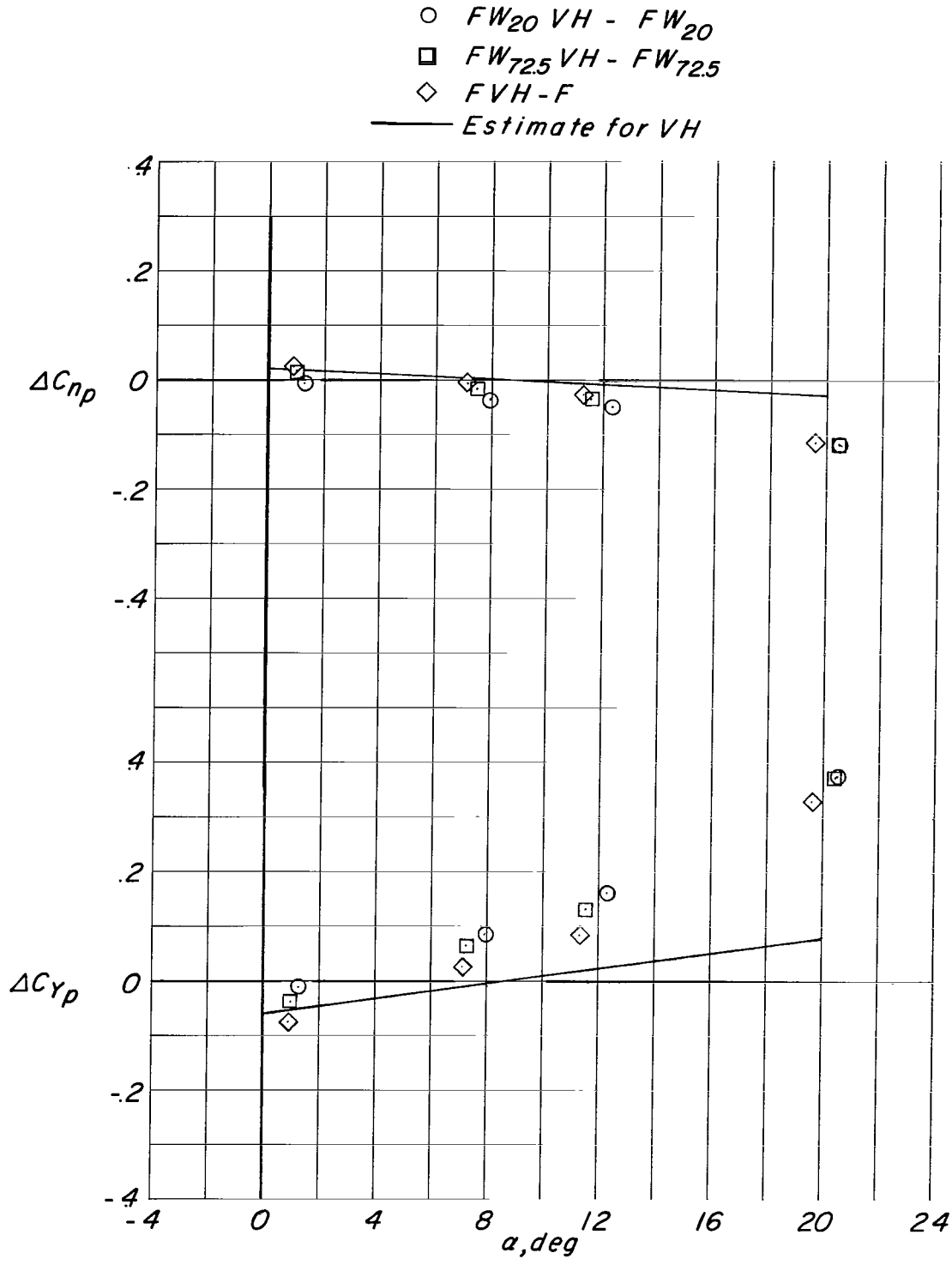

Figure 29.- Contribution of vertical and horizontal tails to C_{n_p} and C_{Y_p}.

NASA-Langley, 1967 L-5155

"The aeronautical and space activities of the United States shall be conducted so as to contribute . . . to the expansion of human knowledge of phenomena in the atmosphere and space. The Administration shall provide for the widest practicable and appropriate dissemination of information concerning its activities and the results thereof."

—NATIONAL AERONAUTICS AND SPACE ACT OF 1958

NASA SCIENTIFIC AND TECHNICAL PUBLICATIONS

TECHNICAL REPORTS: Scientific and technical information considered important, complete, and a lasting contribution to existing knowledge.

TECHNICAL NOTES: Information less broad in scope but nevertheless of importance as a contribution to existing knowledge.

TECHNICAL MEMORANDUMS: Information receiving limited distribution because of preliminary data, security classification, or other reasons.

CONTRACTOR REPORTS: Technical information generated in connection with a NASA contract or grant and released under NASA auspices.

TECHNICAL TRANSLATIONS: Information published in a foreign language considered to merit NASA distribution in English.

TECHNICAL REPRINTS: Information derived from NASA activities and initially published in the form of journal articles.

SPECIAL PUBLICATIONS: Information derived from or of value to NASA activities but not necessarily reporting the results of individual NASA-programmed scientific efforts. Publications include conference proceedings, monographs, data compilations, handbooks, sourcebooks, and special bibliographies.

Details on the availability of these publications may be obtained from:

SCIENTIFIC AND TECHNICAL INFORMATION DIVISION

NATIONAL AERONAUTICS AND SPACE ADMINISTRATION

Washington, D.C. 20546